Organic & Biomolecular Chemistry

ROYAL SOCIETY OF CHEMISTRY

PAPER

View Article Online
View Journal | View Issue

Cite this: *Org. Biomol. Chem.*, 2021, **19**, 8281

Facilitating functionalization of benzene-1,3,5-tricarboxamides by switching amide connectivity†

Sandra M. C. Schoenmakers,‡ Bart W. L. van den Bersselaar,‡ Shikha Dhiman, Lu Su and Anja R. A. Palmans *

Synthetic water-compatible supramolecular polymers based on benzene-1,3,5-tricarboxamides (BTAs) have attracted a lot of interest in recent years, as they are uniquely suited to generate functional multicomponent biomaterials. Their morphologies and intrinsic dynamic behaviour mimic fibrous structures found in nature. Moreover, their modularity allows control of the density of functionalities presented on the surface of the fibres when using functionalized BTA monomers. However, such moieties generally comprise a functionality on only one of three side chains, resulting in lengthy synthetic protocols and limited yields. In this work, we avert the need for desymmetrization of the core by starting from commercially available 5-aminoisophthalic acid. This approach eliminates the statistical reactions and reduces the number of synthetic steps. It also leads to the inversion of the connectivity of one of the amides to the benzene core. By combining spectroscopy, light scattering and cryogenic transmission electron microscopy, we confirm that the inversed amide BTAs (iBTAs) form intermolecular hydrogen bonds and assemble into supramolecular polymers, like previously used symmetrical BTAs, albeit with a slight decrease in water solubility. Solubility problems were overcome by incorporating iBTAs into conventional BTA-based supramolecular polymers. These two-component mixtures formed supramolecular fibres with a morphology and dynamic behaviour similar to BTA-homopolymers. Finally, iBTAs were decorated with a fluorescent dye to demonstrate the synthesis of functional monomers, and to visualize their co-assembly with BTAs. Our results show that functionality can be introduced into supramolecular polymers with monomers that slightly differ in their core structure while maintaining the structure and dynamics of the fibres.

Received 12th August 2021,
Accepted 7th September 2021

DOI: 10.1039/d1ob01587g

rsc.li/obc

Introduction

Nature uses supramolecular interactions to create dynamic and adaptive systems from several structurally diverse building blocks.[1–4] Synthetic water-compatible supramolecular polymers have recently emerged as potential biomaterials since their structure and dynamics can mimic the fibrous structures found in nature.[5,6] The use of non-covalent interactions allows control of the number of biological recognition motifs presented on the supramolecular structures by mixing in different functional monomers in the desired ratio.[7,8] This modular approach has been applied in, for example, supramolecular polymers formed by peptide amphiphiles to create scaffolds for cartilage[9] and bone regeneration,[10] for targeted therapy for atherosclerosis[11] and for the promotion of angiogenesis.[12] In addition, supramolecular polymers based on ureido-pyrimidinones (UPys) showed tuneable dynamics by mixing mono- and bivalent variants.[13] Both types of monomers were functionalized with charged end groups for the intracellular delivery of siRNA[14] and with peptides to make the polymers suitable for cell adhesion.[15] Finally, the periphery of various columnar structures formed by discotic molecules were decorated with carbohydrates to trigger cellular uptake[16,17] and with biotin to create a fibrous scaffold for protein binding.[18,19]

The self-assembly of discotic benzene-1,3,5-tricarboxamides (BTAs) into supramolecular polymers has been studied extensively in recent years.[20] The amides can be connected to the benzene ring *via* the carbonyl group or *via* the nitrogen atom, yielding *C*-centred and *N*-centred BTAs, respectively. Although both variants self-assemble in organic media, the aggregation and hydrogen bonding was weaker in case of *N*-centred BTAs.[21,22] *C*-Centred BTAs have been modified to be compatible with water by decorating the core amides with a hydrophobic chain of at least eleven carbon atoms to protect the intermolecular hydrogen bonds from interaction with the

Laboratory of Macromolecular and Organic Chemistry, Institute for Complex Molecular Systems, Eindhoven University of Technology, Eindhoven, The Netherlands. E-mail: a.palmans@tue.nl

†Electronic supplementary information (ESI) available: Experimental section, synthetic procedures for sidechains and **BTA-C_{11}-EG_4**, supporting spectroscopy and microscopy images, details of the HDX-MS analysis, ^{1}H and ^{13}C NMR spectra of all new compounds. See DOI: 10.1039/d1ob01587g

‡These authors contributed equally to this work.

solvent.[23,24] Their water-solubility was ensured by a tetra(ethylene glycol) periphery (**BTA-C_{11}-EG_4** & **BTA-C_{12}-EG_4**, Chart 1).[23,24] The micrometre long supramolecular fibres that formed in water were found to be highly dynamic[25,26] and the dynamic exchange of monomers between supramolecular polymers could be tuned by modification of the hydrophilic/hydrophobic balance of the monomers[25] or by co-assembling structurally different monomers.[27] Recently, these BTA-based supramolecular polymers have been functionalized with benzoxaborole to interact with red blood cells,[28] with charged groups for the intracellular delivery of siRNA,[29] with carbohydrates for binding to lectins[30] and with DNA for protein recruitment.[31] These examples illustrate the potential use of BTA-based polymers to access sophisticated biomaterials.

Linear peptide amphiphiles and UPy monomers generally contain only one side that is suitable for functionalization, whereas the discotic molecules comprise a C_3-symmetrical core containing three reactive sites for the attachment of functional groups. As it is often favourable to use monovalent monomers to prevent solubility issues and unfavourable steric effects,[28,32] this inherently introduces lengthy synthesis protocols for the desymmetrization of the monomers, often affording limited yields. For *C*-centred BTAs, this involves the statistical deprotection of a trimethyl 1,3,5-benzenecarboxylate core, creating multiple by-products which limits the yield.[33] A strategy to circumvent statistical reactions and to introduce one different side arms onto the core is to start from a C_2-symmetrical core.[34–41] The group of Bouteiller synthesized *N*-substituted benzene-1-urea-3,5-biscarboxamide (BUBA) monomers with a significantly enhanced yield, starting from a commercially available dimethyl 5-aminoisophthalate core.[42] The BUBA molecules showed cooperative self-assembly into long helices in organic media, similar to BTAs. Despite the altered hydrogen-bonding ability of the urea moieties compared to the amides, the BUBA molecules were readily incorporated into the symmetrical BTA-based supramolecular polymers.

Inspired by the work of Bouteiller *et al.*,[42] we here selectively introduce function onto water-compatible BTAs by starting from a C_2-symmetrical 5-aminoisophthalic acid core. This affords a BTA core with the connectivity of one of the amides inverted from *C*-centred to *N*-centred, which we refer to as iBTA. First, we evaluate if this single inversion of amide connectivity affects the supramolecular self-assembly behaviour by synthesizing two unfunctionalized iBTAs. The aqueous self-assembly of iBTAs with an undecyl (**iBTA-C_{11}-EG_4**, Chart 1) and dodecyl aliphatic chains (**iBTA-C_{12}-EG_4**, Chart 1) is compared to their *C*-centred counterparts using UV and Fourier transform infrared (FT-IR) spectroscopy, static light scattering (SLS), cryogenic transmission electron microscopy (cryoTEM) and hydrogen/deuterium exchange followed by mass spectrometry (HDX-MS). Furthermore, we explore the incorporation of iBTAs into supramolecular polymers of BTAs. Finally, we report the synthesis of an iBTA functionalized with a cyanine dye (**iBTA-C_{12}-E_4-Cy3**, Chart 1) and visualise its co-assembly with a *C*-centred BTA using stochastic optical reconstruction microscopy (STORM).[43–47] High resolution microscopy images show that the synthetically easily accessible iBTAs can indeed be used for the introduction of function into BTA-based supramolecular polymers.

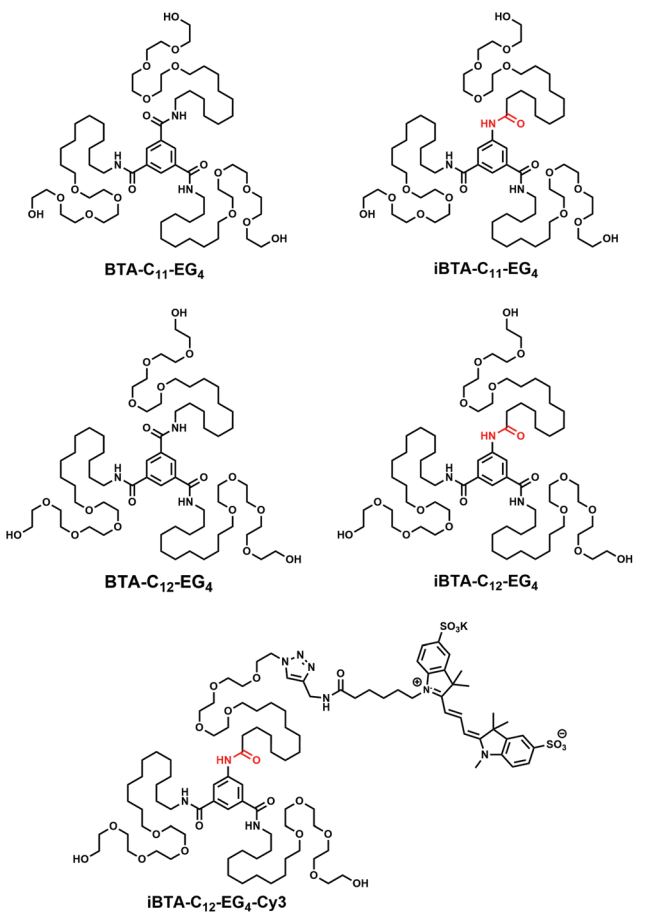

Chart 1 Chemical structures of **BTA-C_{11}-EG_4**, **iBTA-C_{11}-EG_4**, **BTA-C_{12}-EG_4**, **iBTA-C_{12}-EG_4** and **iBTA-C_{12}-EG_4-Cy3**. The inversed amide bonds are indicated in red.

Results and discussion

Design and synthesis of iBTAs

Non-functional iBTAs (Chart 1) were designed to be atomically identical to their C_3-symmetrical counterparts, but differ in the connectivity of one amide bond. The synthesis of iBTAs starts from 5-aminoisophthalic acid or dimethyl 5-aminoisophthalate. For **iBTA-C_{11}-EG_4** and **iBTA-C_{12}-EG_4**, the side chains consist of an aliphatic spacer (undecyl and dodecyl, respectively) to provide a hydrophobic pocket which protects the hydrogen bonds between the amides of the cores,[24] connected to tetra(ethylene glycol) to provide water compatibility.[23] In **iBTA-C_{12}-EG_4-Cy3**, the side chain that is attached to the amine is decorated with a fluorescent sulfonated Cyanine3-dye (sulfo-Cy3) that permits STORM imaging. Hereby the possibility to exploit the desymmetrised core for the controlled introduction of function on only one side chain of the monomer is illustrated.

The synthesis of the iBTAs requires side chains comprising either an amine or a carboxylic acid group for coupling to the core. Amine-terminated side chains (**7a/b**, Scheme S1 and section 2 of the ESI†) were synthesized based on optimized literature procedures.[23] For the carboxylic acid-terminated chains (**11a/b**, Scheme S2 and section 3 of the ESI†), a new synthetic procedure was developed. Herein, a carboxylic acid is protected with a *tert*-butyl group to limit transesterification reactions (Fig. S1, ESI†). A subsequent Williamson ether synthesis with tetra(ethylene glycol) and deprotection of the carboxylic acid yields the desired side chain (**11a/b**). The desired iBTAs can be obtained *via* two pathways, which are demonstrated in the synthesis of both **iBTA-C_{11}-EG_4** and **iBTA-C_{12}-EG_4**. **iBTA-C_{11}-EG_4** was synthesized by attaching the carboxylic acid terminated side chain (**11a**) to dimethyl 5-aminobenzene-1,3-dicarboxylate. After hydrolysis of the methyl esters, the diacid (**16**) was reacted with the amine terminated side chains (**7a**) (Scheme S3 and section 4 of the ESI†) yielding pure **iBTA-C_{11}-EG_4** as confirmed by NMR (Fig. S2 and 3, ESI†), FT-IR and LC-MS. In the second pathway for the synthesis of **iBTA-C_{12}-EG_4** (Scheme 1), the amine terminated side chains (**7b**) were attached first to 5-aminobenzene-1,3-dicarboxylic acid after activation of the carboxylic acids using thionyl chloride. The resulting intermediate (**1**) was stable under argon in the fridge. For **iBTA-C_{12}-EG_4** the synthesis was continued by coupling of the carboxylic acid terminated side chain (**11b**) to **1** resulted in a benzyl protected iBTA (**2**) which after hydrogenation yielded **iBTA-C_{12}-EG_4** in high purity as confirmed by NMR (Fig. S4 and 5, ESI†), FT-IR and LC-MS.

We selected a peripheral azide moiety to introduce a functional group onto the iBTA scaffold, as this allows to directly attach different types of functionalities *via* copper(I)-catalysed azide–alkyne cycloaddition (CuAAC) or *via* a Staudinger reduction of the azide to yield a reactive primary amine. The carboxylic acid terminated side chain was therefore equipped with an azide-derivative of tetra(ethylene glycol) that was synthesized according to a literature procedure.[48] The azide group in the periphery required a minor adaptation of the synthetic route, since azides are known to form side products in a catalytic hydrogenation due to imine formation.[49] Although ammonia can be added to prevent the formation of the intermediate, the catalytic hydrogenation is also effectively hindered by this addition.[50] Therefore, **1** was catalytically hydrogenated to **3** prior to the introduction of the azide-decorated side chain (**14**, Scheme 1). The azide-decorated **iBTA-C_{12}-EG_4-N_3** (**4**) was obtained in high purity as confirmed by NMR (Fig. S6 and 7, ESI†), FT-IR and LC-MS. Finally, **iBTA-C_{12}-EG_4-N_3** was reacted with an alkyne functionalized sulfo-Cy3-dye in a CuAAC reaction to yield **iBTA-C_{12}-EG_4-Cy3** as confirmed by LC-MS.

Supramolecular polymerization of iBTA-C_{11}-EG_4 and iBTA-C_{12}-EG_4 in water

We applied a previously optimised sample preparation protocol to assess the self-assembly of the newly synthesized iBTA monomers into supramolecular polymers.[25] Using this protocol, a clear solution was obtained for **iBTA-C_{11}-EG_4** after overnight equilibration (Fig. S8A, ESI†) but the sample with **iBTA-C_{12}-EG_4** was turbid, indicating that the material did not completely dissolve. To compensate for the decreased solubility in water of **iBTA-C_{12}-EG_4**, the compound was injected into water from a concentrated stock solution in acetonitrile (ACN), followed by controlled heating and cooling of the sample as described before. A final concentration of 10 vol% of ACN in H_2O was required to obtain samples that did not show any scattering (Fig. S8B, ESI†).

The self-assembly of the iBTAs in aqueous media was first studied with UV spectroscopy. We previously established that **BTA-C_{11}-EG_4** and **BTA-C_{12}-EG_4** form micrometre long supramolecular polymers, with characteristic absorbance bands at 211 and 226 nm (Fig. 1A). In contrast, the UV spectra of iBTAs are red shifted, with **iBTA-C_{11}-EG_4** showing a maximum (λ_{max}) at 237 nm and **iBTA-C_{12}-EG_4** at 230 nm. Both spectra also contain

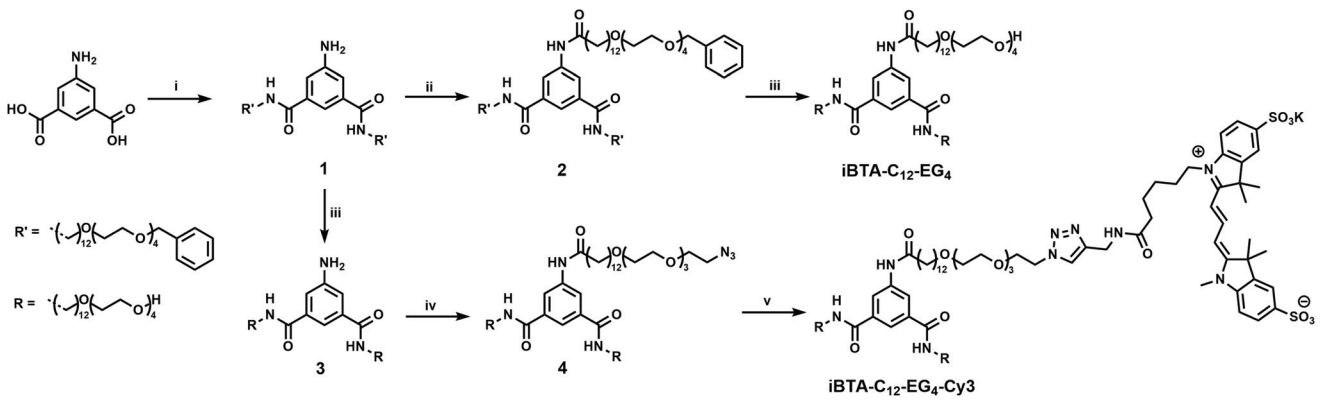

Scheme 1 Synthesis of **iBTA-C_{12}-EG_4** and **iBTA-C_{12}-EG_4-Cy3**. Reagents and conditions: (i) (1) $SOCl_2$, reflux, 2 h. (2) $H_2N(CH_2)_{12}O(CH_2CH_2O)_4OCH_2Ph$ (**7b**), NEt_3, THF, room temperature, 24 h (25%); (ii) (1) $HOOC(CH_2)_{12}O(CH_2CH_2O)_4CH_2Ph$ (**11b**), $(COCl)_2$, DMF, DCM, room temperature, 3 h. (2) NEt_3, room temperature, 24 h (74%); (iii) H_2, 10% Pd/C, MeOH, room temperature, 24 h (**iBTA-C_{12}-EG_4**: 80%; **3**: 80%); (iv) $HOOC(CH_2)_{12}O(CH_2CH_2O)_3CH_2CH_2N_3$ (**14**), DMT-MM, MeOH, room temperature, 24 h (25%); (v) Sulfo-Cy3-alkyne, $CuSO_4$, sodium ascorbate, DMSO, room temperature, 24 h (quant.).

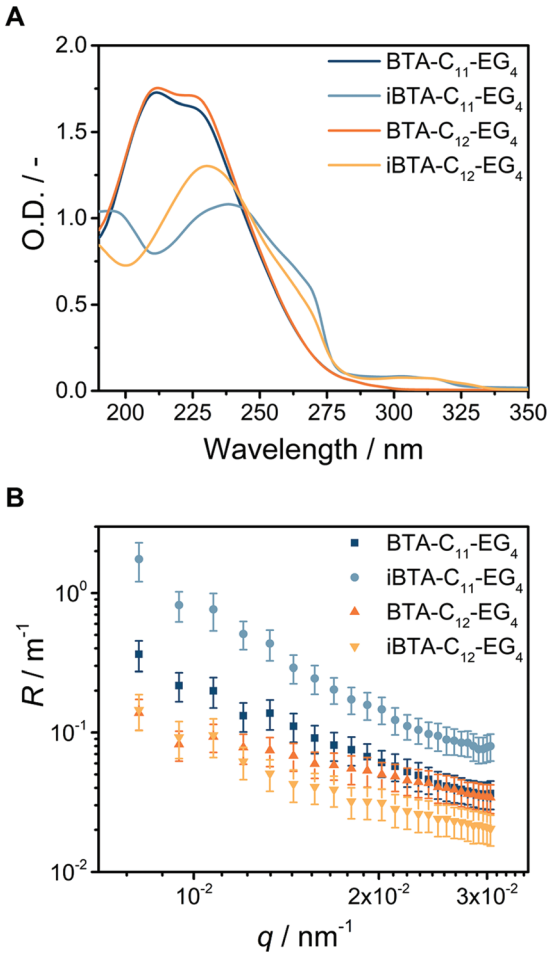

Fig. 1 (A) UV spectra of **BTA-C_{11}-EG_4**, **iBTA-C_{11}-EG_4**, **BTA-C_{12}-EG_4** and **iBTA-C_{12}-EG_4** in water (c = 500 μM, l = 1 mm, T = 20 °C, 10 vol% ACN was present in the sample of **iBTA-C_{12}-EG_4**). (B) Rayleigh ratio R *versus* the scattering vector q as calculated from light scattering experiments with **BTA-C_{11}-EG_4**, **iBTA-C_{11}-EG_4**, **BTA-C_{12}-EG_4** and **iBTA-C_{12}-EG_4** in water (c = 500 μM, l = 1 cm, λ = 532 nm, T = 20 °C, 10 vol% ACN was present in the sample of **iBTA-C_{12}-EG_4**).

a shoulder around 268 nm and a broad band of low intensity between 290–310 nm. The spectra of both iBTA in aqueous media differ significantly compared to those in pure ACN, a solvent in which they are molecularly dissolved (Fig. S8, ESI†). This indicates that iBTAs self-assemble in water. The small differences in λ_{max} between **iBTA-C_{11}-EG_4** and **iBTA-C_{12}-EG_4** probably result from the presence of 10% ACN in the latter, which may affect the propensity to form intermolecular hydrogen bonds.[51] The broad band between 290–310 nm has previously been observed for symmetrical *N*-centred BTAs in organic media[21] and is connected to the switch in connectivity of one amide bond. The spectra of the iBTAs differ both in shape and intensity compared to their symmetrical BTA counterparts, which suggests that the inversion of one of the amides may affect the packing of the hydrogen bonds.

To study the morphologies formed by **iBTA-C_{11}-EG_4** and **iBTA-C_{12}-EG_4** in water, SLS and cryoTEM measurements were performed and compared to those of the symmetrical counterparts **BTA-C_{11}-EG_4** and **BTA-C_{12}-EG_4**. Like **BTA-C_{11}-EG_4** and **BTA-C_{12}-EG_4**, **iBTA-C_{11}-EG_4** and **iBTA-C_{12}-EG_4** show an angular dependence of the Rayleigh ratio R that is typical for the presence of long, elongated structures (Fig. 1B). **iBTA-C_{11}-EG_4** and **iBTA-C_{12}-EG_4** show similar slopes, although the Rayleigh ratio was slightly increased for **iBTA-C_{11}-EG_4** compared to **iBTA-C_{12}-EG_4**. These findings suggest that iBTAs form elongated structures with a similar anisotropy as their symmetrical counterparts, but they differ in size. CryoTEM was used to visualize the morphologies of the iBTAs. The cryoTEM image of **iBTA-C_{11}-EG_4** shows fibres of several micrometres in length (Fig. 2A and Fig. S9, ESI†), whereas the image of **iBTA-C_{12}-EG_4** shows fibres of various lengths, mainly below one micrometre (Fig. 2B and Fig. S10, ESI†). There are, however, subtle differences compared to the morphologies formed by symmetrical BTAs. Both *C*-centred BTAs assemble into micrometre long supramolecular polymers (Fig. S11, ESI†) and for **BTA-C_{12}-EG_4** a double helix structure was recently revealed with high magni-

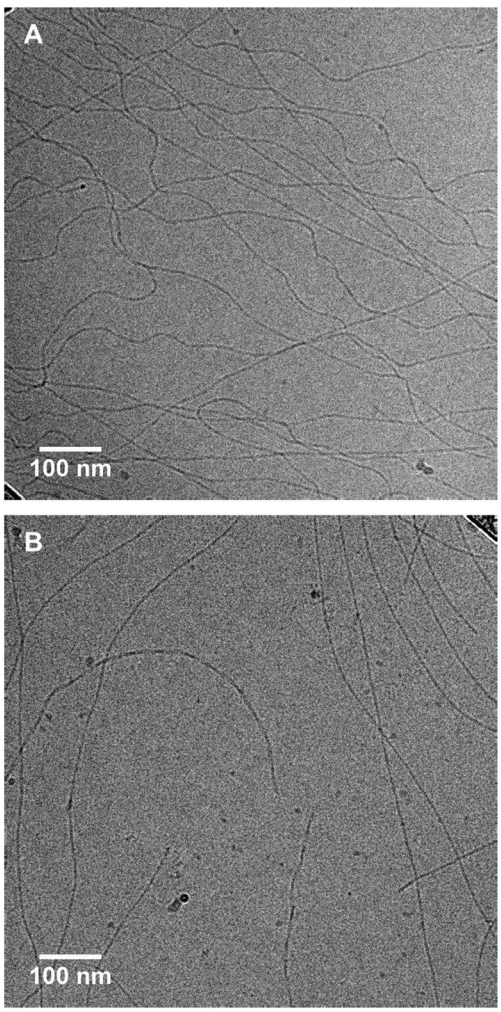

Fig. 2 CryoTEM images of (A) **iBTA-C_{11}-EG_4** and (B) **iBTA-C_{12}-EG_4** in water (c = 500 μM, 10 vol% ACN was present in the sample of **iBTA-C_{12}-EG_4**) at a magnification of 24000×.

fication cryoTEM and image reconstruction,[52] whereas such a strand separation is absent in **BTA-C_{11}-EG_4** (Fig. S11A, ESI†). **iBTA-C_{11}-EG_4** also lacks the strand separation of a double helix structure (Fig. S9B, ESI†), whereas in the case of **iBTA-C_{12}-EG_4** only a fraction of the fibres shows strand separation that may indicate the presence of a double helix (Fig. S10B, ESI†). From these results, we conclude that **iBTA-C_{11}-EG_4** forms fibres of similar morphology as **BTA-C_{11}-EG_4**, and **iBTA-C_{12}-EG_4** forms fibres that are slightly altered in length and secondary structure compared to **BTA-C_{12}-EG_4**. The decrease in length does not originate from the presence of ACN and is solely a result of the amide bond inversion. Further research with high magnification cryoTEM and image reconstruction should be done to confirm these findings.

The properties of the supramolecular polymers were further studied with spectroscopic techniques. FT-IR spectroscopy permits investigation of the presence of intermolecular hydrogen bonds in solution. The C_3-symmetrical BTAs show an amide I vibration (C=O stretch) at 1648 cm^{-1} in the molecularly dissolved state and a vibration at 1635 cm^{-1} when intermolecular hydrogen bonds are present in D_2O (Fig. S12A and B, ESI†). In the molecularly dissolved state, the amide I vibration of **iBTA-C_{11}-EG_4** and **iBTA-C_{12}-EG_4** was positioned at 1642 cm^{-1} and 1643 cm^{-1}, respectively, with a shoulder around 1670 cm^{-1}. The amide I vibration of both iBTAs was found at 1628 cm^{-1} after self-assembly in aqueous solution and the shoulder shifted to 1667 cm^{-1} (Fig. S12C and D, ESI†). This shift of the amide I vibration to lower wavenumbers after self-assembly is indicative for the formation of intermolecular hydrogen bonds. The split of the amide I vibration in case of the iBTAs could arise from the different connectivity of one of the amides in iBTAs. Although the FT-IR spectra of iBTAs are similar, they are shifted towards lower wavenumbers compared to the BTAs, suggesting a different hydrogen bond pattern and/or strength.

In addition, we used the solvatochromic dye Nile Red (NR) to study the presence of hydrophobic regions in the iBTA-based structures. The emission spectra of NR when it is added to **iBTA-C_{11}-EG_4** show a similar $\lambda_{max,em}$ (613 nm) compared to that of **BTA-C_{11}-EG_4** (615 nm, Fig. S13A, ESI†). In contrast, the emission maximum of NR in **iBTA-C_{12}-EG_4** is red-shifted to 626 nm, compared to that of **BTA-C_{12}-EG_4** (612 nm, Fig. S13B, ESI†) indicative of a more polar environment, possibly a result of the presence of 10% ACN. We infer from this that a hydrophobic pocket is present in **iBTA-C_{11}-EG_4**, whereas a decisive conclusion cannot be drawn for **iBTA-C_{12}-EG_4** due to the presence of 10% ACN.

Taken all together, the above results show that iBTAs form a primary supramolecular structure that is similar to that formed by symmetrical BTAs. Long, elongated fibres stabilised by intermolecular hydrogen bonds, which are surrounded by hydrophobic pockets are formed in aqueous media. The morphologies of iBTAs differ in secondary structure from the well-studied **BTA-C_{12}-EG_4** in the sense that undulations due to a double helix structure are absent in **iBTA-C_{11}-EG_4** and less pronounced in **iBTA-C_{12}-EG_4**. This may affect the exchange dynamics of monomers between polymers.

To assess the exchange dynamics of iBTAs, we measured hydrogen/deuterium exchange followed by mass spectrometry (HDX-MS). With HDX-MS, the exchange of labile hydrogen atoms to deuterium atoms is followed over time after dilution of an aqueous samples into D_2O.[25,26] The three outer hydroxyl hydrogen atoms of BTAs and iBTAs are in direct contact with the solvent and will exchange immediately to deuterium atoms. The three amide hydrogen atoms are contained in the hydrophobic pocket and form hydrogen bonds. As a result, their H/D exchange will mainly occur when the monomers move between polymers and are released into the surrounding D_2O. HDX-MS is therefore a powerful tool to elucidate the rate of monomer exchange between polymers and permits to evaluate if the change in connectivity of one of the amides affects the exchange dynamics of the supramolecular polymers.

After confirming that the nature of the supramolecular polymers does not change upon dilution (Fig. S14, ESI†), all samples were 100-fold diluted into D_2O and the percentage of deuterated analogues was followed over time (Fig. S15 and section 7 of the ESI†). The percentage of fully deuterated molecules can be used to compare the exchange dynamics between the different BTAs and iBTAs (Fig. 3). In all cases, a fast increase of deuteration to BTA6D is observed in the first hour, followed by a more gradual increase. After 48 h, 77% of the **BTA-C_{11}-EG_4** polymers is fully deuterated but the deuteration takes longer for **BTA-C_{12}-EG_4** of which 70% of the molecules is fully deuterated after 72 h. 79% of the **iBTA-C_{11}-EG_4** molecules is completely deuterated after 48 hours and 81% of the **iBTA-C_{12}-EG_4** molecules is completely deuterated after 72 h. The H/D exchange of both iBTAs follows a similar trend, indicating that it is not greatly influenced by the length of the hydrophobic chains. **iBTA-C_{11}-EG_4** initially shows a faster exchange than **BTA-C_{11}-EG_4**, but the percentage of fully deuterated molecules is almost the same after 48 h. The percentage

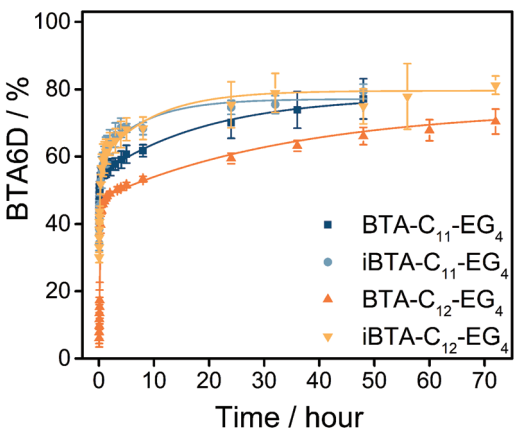

Fig. 3 The percentage of fully deuterated **BTA-C_{11}-EG_4**, **iBTA-C_{11}-EG_4**, **BTA-C_{12}-EG_4** and **iBTA-C_{12}-EG_4** as a function of time after the 100× dilution of 500 μM aqueous samples into D_2O (T = room temperature, 10 vol% ACN was present in the sample of **iBTA-C_{12}-EG_4**). The symbols represent the average and the error bars the standard deviation calculated from three independent measurements. The bi-exponential growth functions were added to guide the eye.

of fully deuterated molecules is higher for **iBTA-C_{12}-EG_4** than for **BTA-C_{12}-EG_4** over the whole period measured. This could indicate that the inversion of the amide bond increases the exchange dynamics, but it could also be an effect of the small percentage of ACN still present after the preparation of the sample.[51] All in all, the exchange dynamics of both iBTAs and BTAs do not show large differences, indicating that the rates of exchange of molecules between polymers is rather similar.

Supramolecular copolymerization of BTA-C_{12}-EG_4 and iBTA-C_{12}-EG_4

The iBTAs have been designed to incorporate functional monomers into supramolecular polymers of BTAs, which requires the co-assembly of BTAs and iBTAs. To evaluate the ability of the molecules to copolymerize, samples of **BTA-C_{12}-EG_4** with several percentages of **iBTA-C_{12}-EG_4** were prepared. **BTA-C_{12}-EG_4** and **iBTA-C_{12}-EG_4** were mixed in the solid state before dissolving in water and applying the heating–cooling protocol as described before. ACN was not required to obtain homogeneous samples, since **BTA-C_{12}-EG_4** helps to solubilize **iBTA-C_{12}-EG_4** indicating their possible copolymerization. UV spectra of mixtures at a concentration of 500 μM do not show any changes in the absorption bands up to 10% of **iBTA-C_{12}-EG_4** (Fig. 4A). At higher percentages of iBTA, a change in the absorption spectra is observed but the spectra never overlap with those of self-sorted systems (Fig. S16A, ESI†), suggesting an interaction between **BTA-C_{12}-EG_4** and **iBTA-C_{12}-EG_4**. The UV spectra indicate that iBTA and BTA form copolymers over a wide range of concentrations (Fig. S16B, ESI†). The formation of supramolecular copolymers of **BTA-C_{12}-EG_4** and **iBTA-C_{12}-EG_4** was further corroborated with SLS (Fig. S17, ESI†), which revealed the presence of structures of similar dimensions as **BTA-C_{12}-EG_4** polymers.

Biomedical applications generally require only a fraction of the monomers within the supramolecular polymers to be functionalized.[28,32] We therefore focus on the supramolecular copolymers containing a maximum of 10% of **iBTA-C_{12}-EG_4**. CryoTEM images verified the formation of the supramolecular copolymers upon mixing **BTA-C_{12}-EG_4** with 10% **iBTA-C_{12}-EG_4** (Fig. 4B). The copolymers are micrometres long and contain the double helix secondary structure as previously observed for **BTA-C_{12}-EG_4** (Fig. S18, ESI†).[52] HDX-MS experiments of the 10% co-assembly confirmed the interaction between **BTA-C_{12}-EG_4** and **iBTA-C_{12}-EG_4** (Fig. S19, ESI†). Additionally, those experiments revealed that the exchange dynamics of the copolymer match with those of the homopolymer of **BTA-C_{12}-EG_4**. From these results, we conclude that the structure and dynamics of **BTA-C_{12}-EG_4** supramolecular polymers are not altered by the incorporation of a small percentage of **iBTA-C_{12}-EG_4**.

Introducing functionalized iBTAs into BTA-based supramolecular polymers

The aforementioned spectroscopic and microscopic experiments confirmed the insignificant changes in structure and monomeric packing between BTA and iBTA by inversion of one of the amide bonds. Although these experiments suggest copolymerization of BTA and iBTA, STORM was used to obtain

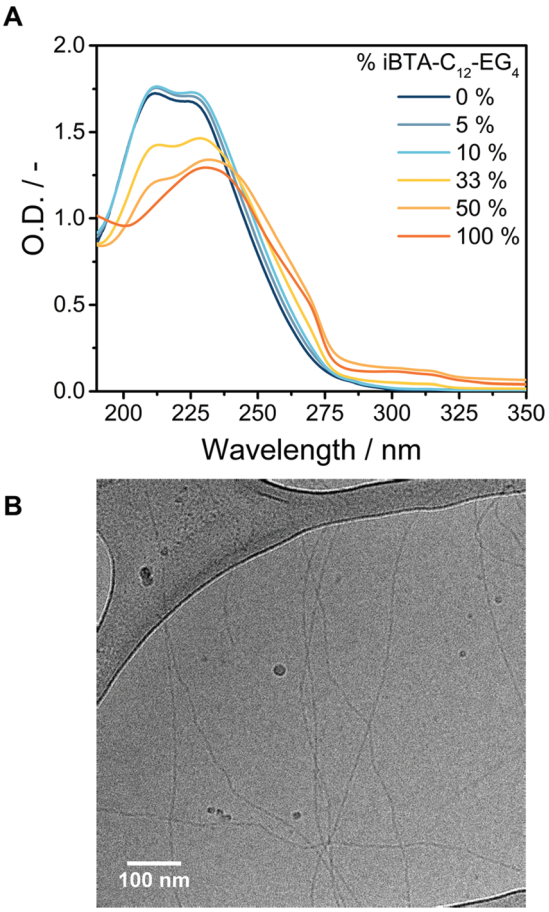

Fig. 4 (A) UV spectra of mixtures of **BTA-C_{12}-EG_4** and **iBTA-C_{12}-EG_4** in different ratios in water (c = 500 μM, l = 1 mm, T = 20 °C). (B) CryoTEM image of the mixture of **BTA-C_{12}-EG_4** with 10% **iBTA-C_{12}-EG_4** in water (c = 500 μM) at a magnification of 24 000×. The dark spherical objects are crystalline ice particles.

visual confirmation for the incorporation of iBTA monomers into **BTA-C_{12}-EG_4** fibres. Hereto, iBTA was functionalized with the fluorescent dye sulfo-Cy3 (**iBTA-C_{12}-EG_4-Cy3**). Dye-functionalized iBTA forms fibrous structures when mixed with **iBTA-C_{12}-EG_4** as evidenced by cryoTEM (Fig. S20 and 21, ESI†). Our main interest is, however, to corroborate if **iBTA-C_{12}-EG_4-Cy3** can introduce its functionality into fibres of **BTA-C_{12}-EG_4**. For this, a sample was prepared of supramolecular copolymers based on **BTA-C_{12}-EG_4** with 10% **iBTA-C_{12}-EG_4-Cy3** incorporated. Additionally, 5% **BTA-C_{12}-EG_4-Cy5** was added for visualization of the polymers of **BTA-C_{12}-EG_4** to confirm that the dye-labelled iBTAs co-assemble with **BTA-C_{12}-EG_4** polymers and to rule out self-sorting of the iBTAs (see Fig. 5A for chemical structures relevant to this experiment). To avoid degradation of the dye at higher temperatures, the samples were prepared by few additional steps after the heating–cooling protocol (section 1, ESI†). The sample was equilibrated for several days, diluted into PBS and adsorbed on a coverslip. Dual channel imaging was performed by simultaneous excitation of Cy3 (green) and Cy5 (red). Normal resolution total internal reflection fluo-

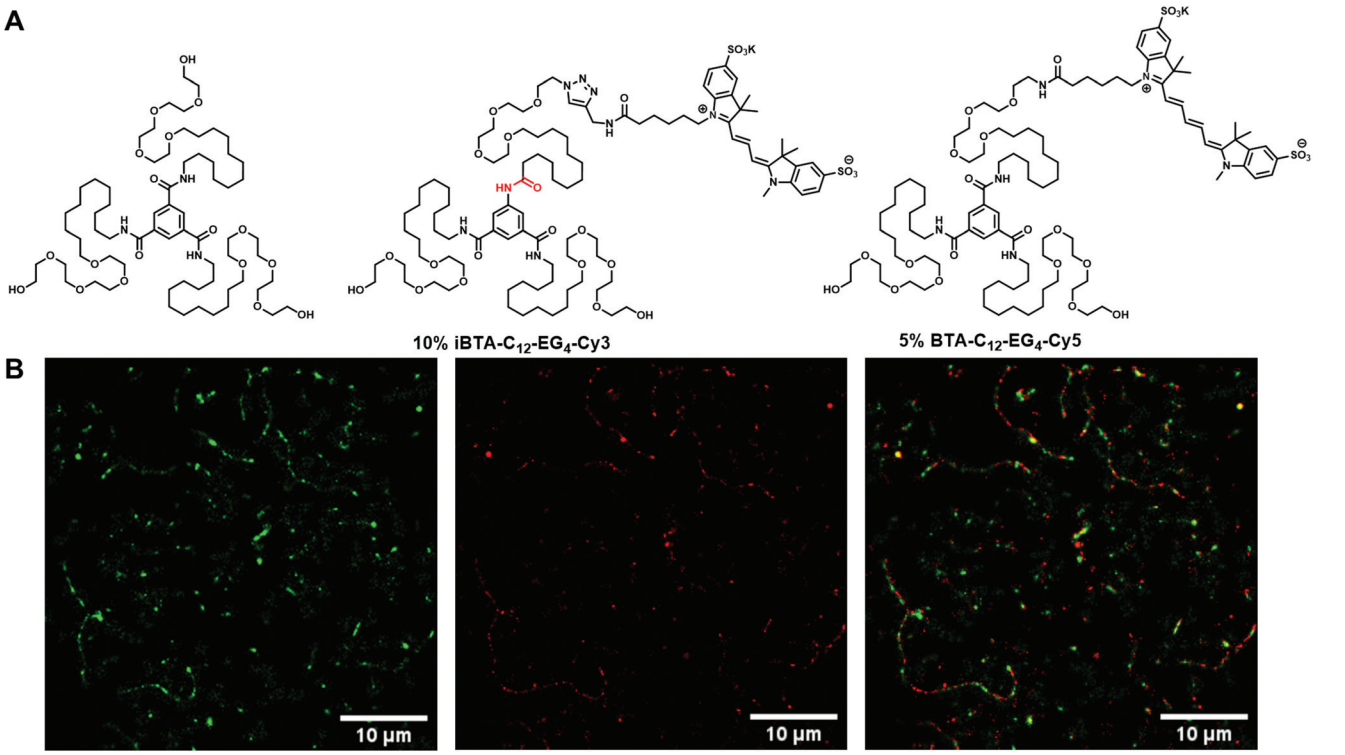

Fig. 5 STORM experiment of a BTA polymer functionalized with iBTA. (A) Chemical structures of the components used in this experiment. A polymer of **BTA-C_{12}-EG_4** was mixed with 10% **iBTA-C_{12}-EG_4-Cy3** and 5% **BTA-C_{12}-EG_4-Cy5**. (B) STORM image of **BTA-C_{12}-EG_4** mixed with dye-functionalized iBTA and BTA. The separate Cy3 (λ_{ex} = 561 nm, green colour) and Cy5 (λ_{ex} = 647 nm, red colour) channels and the merged image are presented.

rescence (TIRF) microscopy and super resolution STORM imaging reveal micrometre long supramolecular polymers that contain both Cy3- and Cy5-labeled monomers (Fig. 5B), thereby confirming that the functionalized iBTA is present within the supramolecular polymers of **BTA-C_{12}-EG_4** (see Fig. S22 and 23 for additional images, ESI†).

Conclusions

In conclusion, we demonstrated the synthesis of iBTAs by starting from a C_2-symmetrical core to facilitate access to BTA-based supramolecular polymers that can be easily appended with a tuneable amount of functional groups. Hereto, we changed the terminal group of one of the side chains from an amine to a carboxylic acid, which required the same amount of synthetic steps and thus did not affect the synthetic effort. Furthermore, an azide moiety—acting as a handle for further functionalisation—was introduced in a three step synthesis similar to the procedure for an amine terminated side chain. By using a carboxylic acid terminated side chain in combination with C_2-symmetrical 5-aminoisophtlalic acid, the statistical deprotection of trimethyl benzene-1,3,5-tricarboxylate was circumvented. The synthetic effort to obtain the desired core molecule was hereby reduced from 6 steps to 3 steps. Although the overall yield of the novel route is slightly lower than that of the previously reported method, we expect these yields to be improved upon further optimization of the reaction conditions.

Since this newly developed synthesis protocol results in the inversion of the connectivity of one of the amide bonds, we first studied if this mutation would hamper the self-assembly of the iBTAs with unfunctional monomers. **iBTA-C_{11}-EG_4** forms supramolecular polymers of similar morphology and dynamics as its *C*-centred counterpart. **iBTA-C_{12}-EG_4**, on the other hand, shows a reduced water solubility compared to **BTA-C_{12}-EG_4**, although they are atomically identical. By adding ACN as a cosolvent, the solubility is enhanced while the formation of supramolecular polymers is retained. The difference in solubility between **iBTA-C_{11}-EG_4** and **iBTA-C_{12}-EG_4**, which differ by one methylene unit only, illustrates once more the importance of the delicate balance between hydrophobic and hydrophilic interactions that should be taken into consideration in the design of new supramolecular building blocks.

Despite their different amide bond orientation, iBTAs are fully compatible with symmetrical BTAs and the molecules were copolymerised in several ratios without the need for a cosolvent. Especially at lower percentages of iBTA, which is desired for the introduction of biological motifs, the copolymers adopt a morphology and exchange dynamics identical to homopolymers of

the BTA. Visual proof of the co-assembly was provided by STORM microscopy of a dye-functionalized **iBTA-C_{12}-EG_4**.

Our results exemplify that iBTAs are a versatile platform for the functionalization of BTA-based polymers without altering the properties of the polymers. We envision that the introduction of function *via* building blocks with a small mismatch in core structure is not restricted to the BTA-based system presented here and this strategy should be applied to other building blocks used in the quest towards multipurpose synthetic biomaterials. Our future work will focus on the interaction of functional iBTAs embedded in BTA-based systems with biological material.

Experimental

Materials and methods

BTA-C_{11}-EG_4,[24] **BTA-C_{12}-EG_4**[23] and **BTA-C_{12}-EG_4-Cy5**[45] were synthesized according to literature procedures. All reagents and chemicals used were obtained from commercial sources at the highest purity available and used without further purification. All solvents were of AR quality and purchased from Biosolve. Deuterated compounds were obtained from Cambridge Isotope Laboratories and stored over 4 Å molecular sieves. Dry solvents were obtained using MBraun solvent purification system (MB SPS-800). Water for aqueous samples was purified on an EMD Millipore Milli-Q Integral Water Purification System. Glassware was dried in an oven at 135 °C overnight prior to reactions under dry conditions. Reactions were followed by thin-layer chromatography (TLC) using 60-F_{254} silica gel plates from Merck and visualized by UV light at 254 nm and/or staining (ninhydrin, bromocresol green, potassium permanganate, iodine chamber). Flash column chromatography was performed on a Grace Reveleris X2 chromatography system using Reveleris Silica Flash cartridges. Reversed phase column chromatography was achieved using a reversed phase KP-C_{18}-HS SNAP column or a Reveleris C_{18} reversed-phase flash cartridge. All ^{1}H NMR and ^{13}C NMR spectra were recorded on Bruker Ultrashield spectrometers (400 MHz for ^{1}H NMR and 100 MHz for ^{13}C NMR). Proton chemical shifts are reported in ppm (δ) downfield from trimethyl silane (TMS) using the resonance frequency of the deuterated solvent ($CDCl_3$; 7.26 ppm, DMSO-d_6; 2.50 ppm) as the internal standard. Peak multiplicities are abbreviated as s: singlet; d: doublet; m: multiplet; t: triplet, p: pentet, dd: double doublet. Carbon chemical shifts are reported in ppm (δ) downfield from TMS using the resonance frequency of the deuterated solvents ($CDCl_3$; 77.16 ± 0.06 ppm; DMSO-d_6; 39.52 ± 0.06 ppm) as the internal standard. Infrared spectra were recorded using a PerkinElmer Spectrum Two FT-IR spectrometer equipped with a PerkinElmer Universal ATR Two Accessory. All solid-state spectra were measured at room temperature from 500 cm^{-1} to 4000 cm^{-1} and were averaged over 16 scans. Liquid chromatography mass spectroscopy (LC-MS) spectra were acquired using a device consisting of multiple components: Shimadzu SCL-10 A VP system controller with Shimadzu LC-10AD VP liquid chromatography pumps (with an Alltima C_{18} 3 u (50 × 2.1 mm) reversed-phase column and gradients of water), a Shimadzu DGU 20A3 prominence degasser, a Thermo Finnigan surveyor auto sampler, a Thermo Finnigan surveyor PDA detector and a Thermo Scientific LCW Fleet. All samples were dissolved in 1 : 1 H_2O : ACN in *ca.* 0.1 mg mL^{-1} concentration. Matrix assisted laser absorption/ionization mass time of flight mass spectroscopy (MALDI-TOF-MS) spectra were obtained on a Bruker Autoflex Speed. α-Cyano-4-hydroxycinnamic acid (CHCA) or *trans*-2-[3-(4-*tert*-butylphenyl)-2-methyl-2-propenylidene]malononitrile (DCBT) were used as matrices. All samples were dissolved in either DCM or $CHCl_3$ with a concentration of 1.0 mg mL^{-1}.

Synthetic procedures

***tert*-Butyl-12-bromododecanoate (9a).** This procedure was adapted from literature.[53] A round-bottom flask was charged with 12-bromododecanoic acid (1.0609 g, 3.7996 mmol) in dry THF (10 mL) at 0 °C and *tert*-butyl imidate was added (2.0 mL, 11.1 mmol). Consequently, $BF_3{\cdot}OEt_2$ (160.0 μL, 608.0 μmol) was added and the mixture was stirred overnight. The reaction mixture was quenched using saturated aqueous $NaHCO_3$. Ethyl acetate was added and the mixture was washed using saturated $NaHCO_3$ (3×) and brine (1×). The organic phase was dried over $NaSO_4$ and concentrated *in vacuo*. The crude oil was purified using column chromatography (SNAP-KI column 40 g, eluent hexane/ethyl acetate 4.5 CV: 25/1; 4 CV ramp to 4/1; 3.8 CV 4/1) to yield the product as a colourless oil. Yield: 619.2 mg, 47%. ^{1}H NMR (400 MHz, DMSO-d_6 δ): 3.52 (t, J = 6.7 Hz, 2H, $CH_2CH_2C\underline{H}_2Br$), 2.16 (t, J = 7.3 Hz, 2H, *t*BuOOCC$\underline{H}_2$), 1.77 (p, J = 7.0 Hz, 2H, $CH_2C\underline{H}_2CH_2Br$), 1.48 (m, 2H, *t*BuOOCCH_2C$\underline{H}_2$), 1.39 (s, 9H, $\underline{t\text{Bu}}$OOC), 1.24 (s, 12H, aliphatic). ^{13}C NMR (100 MHz, $CDCl_3$ δ): 173.36, 79.90, 63.12, 35.63, 34.06, 32.84, 29.46, 29.42, 29.40, 29.28, 29.09, 28.76, 28.18, 28.13, 25.11. FT-IR (ATR) ν (cm^{-1}): 3459, 3007, 2975, 2926, 2855, 1729, 1457, 1392, 1366, 1255, 1151, 1043, 952, 919, 848, 755, 723, 645, 563, 462.

***tert*-Butyl-13-bromotridecanoate (9b).** The synthesis of **9b** was performed following the same procedure as described for **9a**, yielding **9b** as a colourless oil that solidified upon standing (1.9887 g, 55%). ^{1}H NMR (400 MHz, $CDCl_3$ δ): 3.42–3.39 (t, J = 6.9 Hz, 2H, $CH_2C\underline{H}_2Br$), 2.20 (t, J = 7.5 Hz, 2H, *t*BuOOCC$\underline{H}_2CH_2$), 1.85 (p, J = 7.0 Hz, 2H, C$\underline{H}$2CH$_2$Br), 1.69–1.66 (m, 2H, *t*BuOOCCH_2C$\underline{H}_2$), 1.45–1.36 (m, 11H, $\underline{t\text{Bu}}$OOCCH_2, C$\underline{H}_2CH_2CH_2Br$), 1.36–1.21 (m, 14H, aliphatic). ^{13}C NMR (100 MHz, $CDCl_3$ δ): 173.36, 79.89, 60.40, 35.64, 34.06, 32.85, 29.54, 29.50, 29.45, 29.43, 29.29, 29.10, 28.77, 28.18, 28.13, 25.12. FT-IR (ATR) ν (cm^{-1}): 3424, 2975, 2916, 2850, 1718, 1473, 1366, 1218, 1150, 1108, 847, 718.

***tert*-Butyl-1-phenyl-2,5,8,11,14-pentaoxaheptacosan-26-oate (10a).** A three-necked round bottom flask (250 mL, dried at 135 °C) was charged with monobenzyl tetraethylene glycol (0.8092 mg, 2.8458 mmol) in dry DMF (60 mL) and some 3 Å mole sieves to ensure dry conditions. The solution was cooled to 0 °C and NaH (0.1094 g, 2.7350 mmol) was added, upon which the mixture foamed vigorously. The ice bath was removed and

after 30 minutes, **9a** (0.5978 g, 1.7827 mmol) was added in one portion and the mixture was stirred over the weekend. The mixture was subsequently quenched with H_2O (50 mL) and extracted with diethyl ether (3× 50 mL). Some saturated NaCl was added to improve phase separation. The organic layers were combined, dried with $MgSO_4$, filtered and concentrated *in vacuo*. The crude product was further purified using column chromatography (SNAP-KI column 24 g, eluent heptane/ethyl acetate 3 CV 80/20; 1 CV ramp to 70/30; 6 CV 70/30). The product was obtained as a colourless oil. Yield: 295.0 mg, 31%. ^{1}H NMR (400 MHz, $CDCl_3$ δ): 7.35–7.29 (m, 5H, Ar), 4.57 (s, 2H, $ArCH_2O$), 3.66–3.64 (m, 14H, $O(CH_2)_2O$), 3.58–3.56 (m, 2H, $O(CH_2)_2O$), 3.44 (t, J = 6.8 Hz, 2H, $CH_2CH_2CH_2O$), 2.20 (t, J = 7.5 Hz, 2H, *t*BuOOCCH_2), 1.62–1.52 (m, 4H, *t*BuOOCCH$_2$CH_2 & $CH_2CH_2CH_2O$), 1.44 (s, 9H, *t*BuOOCCH$_2$), 1.35–1.20 (m, 14H, aliphatic). ^{13}C NMR (100 MHz, $CDCl_3$ δ): 173.37, 128.36, 127.75, 127.59, 79.89, 73.25, 71.56, 70.66, 70.62, 70.05, 69.44, 35.64, 31.89, 29.64, 29.59, 29.56, 29.50, 29.48, 29.32, 29.11, 28.13, 26.10, 25.13, 22.71, 14.13. FT-IR (ATR) ν (cm^{-1}): 2925, 2855, 1730, 1455, 1366, 1250, 1144, 1103, 1043, 946, 848, 736, 698, 464.

***tert*-Butyl-1-phenyl-2,5,8,11,14-pentaoxaheptacosan-27-oate (10b).** The synthesis of **10b** was performed following the same procedure as described for **10a**, yielding **10b** as a colourless oil that solidified upon standing. Yield: 535.0 mg, 31%.

^{1}H NMR (400 MHz, $CDCl_3$ δ): 7.35–7.29 (m, 5H, Ar), 4.57 (s, 2H, $ArCH_2O$), 3.66–3.64 (m, 14H, $O(CH_2)_2O$), 3.58–3.56 (m, 2H, $O(CH_2)_2O$), 3.44 (t, J = 6.8 Hz, 2H, $CH_2CH_2CH_2O$), 2.20 (t, J = 7.5 Hz, 2H, *t*BuOOCCH_2), 1.62–1.52 (m, 4H, *t*BuOOCCH$_2$CH_2 & $CH_2CH_2CH_2O$), 1.44 (s, 9H, *t*BuOOCCH$_2$), 1.35–1.20 (m, 16H, aliphatic). ^{13}C NMR (100 MHz, $CDCl_3$ δ): 138.29, 128.35, 127.74, 127.58, 79.88, 77.22, 73.25, 71.56, 70.66, 70.63, 70.06, 69.45, 35.65, 29.65, 29.60, 29.51, 29.32, 29.11, 28.14, 26.10, 25.14. FT-IR (ATR) ν (cm^{-1}): 2922, 2853, 1728, 1455, 1365, 1247, 1148, 1101, 845, 737, 698. LC-MS: *m*/*z* calculated for $C_{32}H_{56}O_7 + Na^+$: 575.39 $[M + Na]^+$; observed 575.42; *m*/*z* calculated for $C_{28}H_{46}O_6 + NH_4^+$: 496.70 [transesterification/elimination product + $NH_4]^+$; observed 496.25 (section 2 of the ESI†).

1-Phenyl-2,5,8,11,14-pentaoxahexacosan-26-oic acid (11a). A round-bottom flask was charged with **10a** (0.2950 g, 0.5475 mmol) was dissolved in DCM (15 mL) and one equivalent TFA was added (15 mL). The mixture was stirred at room temperature overnight. After this, it was quenched at 0 °C with water. The aqueous phase was washed with DCM (3× 20 mL). The combined organic phases were dried over $MgSO_4$ and concentrated *in vacuo*. The product was purified using column chromatography to remove amongst others the alkene side product (SNAP-KI column 24 g eluent heptane/ethyl acetate 80/20–50/50). After this, the compound was fully dried under vacuum with P_2O_5 to yield the pure product as a colourless oil. Yield: 123.7 mg, 81% total. ^{1}H NMR (400 MHz, DMSO-d_6 δ): 11.96 (s, 1H, HOOCCH$_2$), 7.31 (m, 5H, Ar), 4.49 (s, 2H, $ArCH_2O$), 3.60–3.40 (m, 16H, $O(CH_2)_2O$), 3.33 (m, 2H, CH_2CH_2O), 2.18 (t, J = 7.3 Hz, 2H, HOOCCH$_2$CH$_2$), 1.47 (m, 4H, HOOCCH$_2$CH_2 & CH_2CH$_2$O), 1.33–1.15 (m, 14H, aliphatic). ^{13}C NMR (100 MHz, DMSO-d_6 δ): 174.95, 138.95, 128.66, 127.93, 127.81, 72.49, 70.77, 70.28, 69.95, 69.60, 34.15, 31.73, 29.68, 29.49, 29.43, 29.37, 29.22, 29.03, 28.85, 26.12, 24.97, 22.58, 14.43. FT-IR (ATR) ν (cm^{-1}): 3584–2440, 2928, 2852, 1733, 1706, 1456, 1353, 1251, 1096, 938, 845, 735, 698. MALDI-TOF-MS: *m*/*z* calculated for $C_{27}H_{46}O_7 + Na^+$: 505.31 $[M + Na]^+$; observed 505.35; *m*/*z* calculated for $C_{27}H_{46}O_7 + K^+$: 521.42 $[M + K]^+$; observed 521.32.

1-Phenyl-2,5,8,11,14-pentaoxaheptacosan-27-oic acid (11b). The synthesis of **11b** was performed following the same procedure as described for **11a**, yielding **11b** as a colourless oil. Yield: 327.1 mg, 68%. ^{1}H NMR (400 MHz, DMSO-d_6 δ): 11.96 (s, 1H, HOOCCH$_2$), 7.31 (m, 5H, Ar), 4.49 (s, 2H, $ArCH_2O$), 3.60–3.40 (m, 16H, $O(CH_2)_2O$), 3.33 (m, 2H, CH_2CH_2O), 2.18 (t, J = 7.3 Hz, 2H, HOOCCH$_2$CH_2), 1.47 (m, 4H, HOOCCH$_2$CH_2 & CH_2CH$_2$O), 1.33–1.15 (m, 16H, aliphatic). ^{13}C NMR (100 MHz, DMSO-d_6 δ): 174.95, 138.94, 128.65, 127.92, 127.81, 72.49, 70.76, 70.32, 70.28, 70.24, 69.94, 69.60, 34.12, 31.73, 29.67, 29.49, 29.45, 29.37, 29.33, 29.21, 29.01, 26.11, 24.96. FT-IR (ATR) ν (cm^{-1}): 3719–2365, 2921, 2856, 1737, 1703, 1454, 1349, 1242, 1101, 940, 739, 698. MALDI-TOF-MS: *m*/*z* calculated for $C_{28}H_{48}O_7 + Na^+$: 519.33 $[M + Na]^+$; observed 519.33; *m*/*z* calculated for $C_{28}H_{48}O_7 + K^+$: 535.44 $[M + K]^+$; observed 535.30.

***tert*-Butyl-1-azido-3,6,9,12-tetraoxapentacosan-25-oate (13).** A three-necked round-bottom flask was dried at 135 °C and charged with 2-(2-(2-(2-azidoethoxy)ethoxy)ethoxy)ethan-1-ol[48] (**12**) (0.5316 g, 0.0024 mol) and dry DMF (25 mL). The solution was cooled to 0 °C and sodium hydride (0.1195 g, 0.0029 mol) was added to the stirring solution. The reaction mixture was allowed to heat up to room temperature after 30 min and *tert*-butyl-13-bromotridecanoate **8b** (0.5573 g, 0.0016 mol) dissolved in 5 mL DMF was added in one go. The mixture was left to stir overnight and subsequently quenched with H_2O (20 mL) and extracted with diethyl ether (3× 50 mL). A small amount of saturated NaCl was added to improve phase separation. The organic layers were combined, dried with $MgSO_4$, filtered and concentrated *in vacuo*. The crude product was further purified using column chromatography (SNAP-KI column 24 g, eluent heptane/ethyl acetate 80/20–70/30). The product was obtained as a colourless oil. Yield: 221.6 mg, 28%. ^{1}H NMR (400 MHz, $CDCl_3$ δ): 3.66 (m, 12H, $O(CH_2)_2O$), 3.58 (m, 2H, $O(CH_2)_2O$), 3.45 (t, J = 6.8 Hz, 2H, $CH_2CH_2CH_2O$), 3.39 (t, J = 5.1 Hz, 2H, N_3CH_2), 2.20 (t, J = 7.5 Hz, 2H, *t*BuOOCCH$_2$CH$_2$), 1.56 (m, 4H, *t*BuOOCCH$_2$CH_2 & $CH_2CH_2CH_2O$), 1.44 (s, 9H, *t*BuOOCH$_2$), 1.21 (m, 16H, aliphatic). ^{13}C NMR (100 MHz, $CDCl_3$ δ): 79.88, 77.21, 71.56, 70.71, 70.65, 70.06, 50.71, 35.65, 31.89, 29.65, 29.60, 29.49, 29.32, 29.11, 29.03, 28.13, 26.11, 25.13, 22.70, 14.12. FT-IR (ATR) ν (cm^{-1}): 3455, 2922, 2853, 2104, 1729, 1460, 1367, 1247, 1147, 1102, 936, 851. LC-MS: *m*/*z* calculated for $C_{25}H_{49}N_3O_6 + Na^+$: 510.35 $[M + Na]^+$; observed 510.25; *m*/*z* calculated for $C_{21}H_{39}N_3O_5 + Na^+$: 436.28 [transesterification/elimination product + $Na]^+$; observed 436.17 (section 2 of the ESI†).

1-Azido-3,6,9,12-tetraoxapentacosan-25-oic acid (14). A round-bottom flask was charged with **13** and DCM (15 mL) and one equivalent TFA was added (15 mL). The mixture was stirred at room temperature overnight. After this, it was

quenched at 0 °C with water. The aqueous phase was washed with DCM three times. The combined organic phases were dried over $MgSO_4$ and concentrated *in vacuo*. The product was purified using column chromatography (SNAP-KI 24 g, eluent heptane/ethyl acetate 80/20–50/50). The product was obtained as a colourless oil. Yield: 177.9 mg, 90%. ^{1}H NMR (400 MHz, DMSO-d_6 δ): 11.96 (s, 1H, HOOCC$\underline{H}_2$), 3.60–3.40 (m, 16H, O-(C$\underline{H}_2$)$_2$-O), 3.33 (m, 2H, CH$_2$C$\underline{H}_2$O), 2.18 (t, J = 7.3 Hz, 2H, HOOCC$\underline{H}_2$CH$_2$), 1.47 (m, 4H, HOOCCH$_2$C$\underline{H}_2$ & C$\underline{H}_2$CH$_2$O), 1.33–1.15 (m, 16H, aliphatic). ^{13}C NMR (100 MHz, DMSO-d_6 δ): 174.95, 70.77, 70.31, 70.27, 70.18, 69.95, 69.72, 60.22, 50.47, 34.12, 31.73, 29.67, 29.50, 29.45, 29.38, 29.33, 29.21, 29.02, 28.84, 26.12, 24.96, 22.57, 21.22, 14.55, 14.42. FT-IR (ATR) ν (cm^{-1}): 3650–2450, 2924, 2854, 2098, 1731, 1708, 1454, 1349, 1284, 1243, 1102, 931, 837. MALDI-TOF-MS: m/z calculated for $C_{21}H_{41}N_3O_6$ + Na^+: 454.29 $[M + Na]^+$; observed 454.27.

Dimethyl 5-(1-phenyl-2,5,8,11,14-pentaoxahexacosan-26-amido)isophthalate (15). An oven-dried round-bottom flask (dried at 140 °C) was charged with **11a** (0.1214 g, 0.2515 mmol) in DCM (3 mL). Oxalyl chloride (120.0 μL, 1.3 mmol) was added to the stirring mixture. One droplet of DMF was added, after which vigorous bubbling was observed. After ten minutes, a bright yellow colour was observed. The mixture was stirred for three hours, after which it was concentrated *in vacuo*. The purity of the activated acid was confirmed using ^{1}H NMR and it was used without further purification. Subsequently, a two-necked round bottom flask was dried at 140 °C and charged with dimethyl-5-aminoisophthalate (75.3 mg, 0.4 mmol) in dry THF (4 mL). Triethylamine (267.0 μL, 1.9 mmol) was added in one portion and the mixture was stirred for 15 min. The acid chloride was dissolved in dry THF (2 mL) and added dropwise. The mixture was stirred overnight, after which it was concentrated *in vacuo*. The solid was dissolved in chloroform and extracted with water (3× 30 mL). After this, the water phase was washed with chloroform (3× 30 mL) and the combined organic fractions were dried over $MgSO_4$. The mixture was filtered, concentrated *in vacuo* and purified using column chromatography (SNAP-KI column 24 g, eluent heptane/ethyl acetate 50/50) to yield the product as a colourless sticky oil. Yield: 69.7 mg, 41%. ^{1}H NMR (400 MHz, DMSO-d_6 δ): 10.33 (s, 1H, ArN$\underline{H}$COCH$_2$), 8.50 (s, 2H, core next to amide), 8.15 (s, 1H, core between esters), 7.31 (m, 5H, Ar), 4.48 (s, 2H, ArC$\underline{H}_2$O), 3.89 (s, 6H, 2× ArCOOC$\underline{H}_3$), 3.49 (m, 16H, O(C$\underline{H}_2$)$_2$O), 3.34 (m, 2H, CH$_2$C$\underline{H}_2$O), 2.33 (t, J = 7.2 Hz, 2H, NHCOC$\underline{H}_2$CH$_2$), 1.59 (m, 2H, NHCOCH$_2$C$\underline{H}_2$), 1.45 (m, 2H, C$\underline{H}_2$CH$_2$O), 1.27 (m, 14H, aliphatic). ^{13}C NMR (100 MHz, DMSO-d_6 δ): 172.42, 165.77, 140.69, 138.92, 131.08, 128.65, 127.92, 127.80, 124.22, 123.85, 72.47, 70.75, 70.31, 70.26, 70.22, 69.93, 69.58, 60.23, 52.99, 36.86, 31.73, 29.66, 29.47, 29.43, 29.34, 29.21, 29.03, 28.85, 26.11, 25.37, 22.58, 21.24, 14.56, 14.44. FT-IR (ATR) ν (cm^{-1}): 3322, 2925, 2855, 1725, 1698, 1604, 1553, 1453, 1438, 1342, 1240, 1102, 1003, 949, 906, 873, 794, 759, 721, 698, 542, 464. LC-MS: m/z calculated for $C_{37}H_{55}NO_{10}$ + H^+: 674.39 $[M + H]^+$; observed 674.25; m/z calculated for $C_{37}H_{55}NO_{10}$ + NH_4^+: 691.41 $[M + NH_4]^+$; observed 691.17.

5-(1-Phenyl-2,5,8,11,14-pentaoxahexacosan-26-amido)isophthalic acid (16). A round-bottom flask was charged with **15** (69.7 mg, 0.1 mmol) in methanol/isopropanol (2/1, 1.5 mL) and lithium hydroxide monohydrate (19.6 mg, 0.8 mmol) was added, followed by a few drops of water. The reaction mixture was stirred overnight at room temperature and subsequently concentrated *in vacuo*. Water was added to the solids (10 mL) and the mixture was acidified with HCl (1 M) followed by extraction with DCM (3× 30 mL). The organic layers were combined, dried with $MgSO_4$, filtered and concentrated *in vacuo* yielding the product as a white waxy solid. Yield: 67.6 mg, 100%. ^{1}H NMR (400 MHz, DMSO-d_6 δ): 8.22 (s, 2H, core next to amide), 8.12 (s, 1H, core between carboxylic acids), 7.34–7.27 (m, 5H, Ar), 6.31 (s, 2H, 2× COO$\underline{H}$), 4.57 (s, 2H, ArC$\underline{H}_2$O), 3.69–3.56 (m, 16H, O(C$\underline{H}_2$)$_2$O), 3.45–3.38 (m, 2H, CH$_2$CH$_2$C$\underline{H}_2$O), 2.30–2.27 (t, J = 7.3 Hz, 2H, ArNHCOC$\underline{H}_2$CH$_2$), 1.58–1.47 (m, 2H, CH$_2$C$\underline{H}_2$CH$_2$O), 1.47–1.44 (m, 2H, ArNHCOCH$_2$C$\underline{H}_2$), 1.27 (m, 14H, aliphatic). ^{13}C NMR (100 MHz, DMSO-d_6 δ): 181.91, 128.66, 127.93, 72.47, 70.76, 70.26, 69.59, 36.86, 33.68, 32.83, 29.66, 29.49, 26.34, 26.12, 23.06. FT-IR (ATR) ν (cm^{-1}): 3500–2500, 2917, 2855, 1625, 1559, 1435, 1358, 1095, 949, 779, 719, 697. MALDI-TOF-MS: m/z calculated for $C_{35}H_{51}NO_{10}$ + Li^+: 652.29 $[M + Li]^+$; observed 652.39; m/z calculated for $C_{35}H_{51}NO_{10}$ + Na^+: 668.34 $[M + Na]^+$; observed 668.37.

5-(1-Phenyl-2,5,8,11,14-pentaoxahexacosan-26-amido)-N_1,N_3-bis(1-phenyl-2,5,8,11,14-pentaoxapentacosan-25-yl)isophthalamide (17). An oven-dried round-bottom flask (dried at 135 °C) and charged with **16** (67.6 mg, 0.1 mmol) in dry DMF (1 mL). Triethylamine (72.0 μL, 0.5 mmol) and **7a** (113.0 mg, 0.2 mmol) were added to the mixture and it was cooled to 0 °C. Subsequently, TBTU (99.2 mg, 0.3 mmol) was added and the mixture was stirred overnight at room temperature. The mixture was quenched with water, upon which it turned milky-white. The mixture was extracted with ethyl acetate (3× 30 mL) and the combined organic phases were extracted with water and brine. The compound was purified using column chromatography (SNAP-KI column 12 g, eluent isopropanol/DCM, 0/100–5/95–10/90) which yielded the pure product as a slightly yellow solid. Yield: 43.8 mg, 28%. ^{1}H NMR (400 MHz, $CDCl_3$ δ): 8.27 (m, 1H, ArN$\underline{H}$COCH$_2$), 8.24 (s, 2H, core protons), 7.98 (s, 1H, core proton between regular amides), 7.34–7.27 (m, 15H, Ar), 6.52 (m, 2H, 2× ArCON$\underline{H}$CH$_2$), 4.57 (s, 6H, 3× ArC$\underline{H}_2$O), 3.69–3.54 (m, 48H, O(C$\underline{H}_2$)$_2$O), 3.47–3.38 (m, 10H, 3× CH$_2$CH$_2$C$\underline{H}_2$O, 2× CONHC$\underline{H}_2$CH$_2$), 2.43–2.39 (t, J = 7.5 Hz, 2H, ArNHOCC$\underline{H}_2$CH$_2$), 1.73–1.68 (m, 2H, 1.85 ArNHOCCH$_2$C$\underline{H}_2$), 1.60–1.53 (m, 10H, 3× CH$_2$C$\underline{H}_2$CH$_2$O, 2× ArCONHCH$_2$C$\underline{H}_2$), 1.36–1.21 (m, 42H, aliphatic). ^{13}C NMR (100 MHz, $CDCl_3$ δ): 128.36, 127.77, 127.61, 77.23, 73.25, 71.55, 70.60, 70.05, 69.42, 64.47, 38.63, 29.60, 29.58, 29.51, 29.43, 29.36, 29.24, 26.94, 26.06, 25.38. FT-IR (ATR) ν (cm^{-1}): 3320, 2926, 2853, 1648, 1536, 1425, 1349, 1096, 734, 697. LC-MS: m/z calculated for $C_{87}H_{141}N_3O_{18}$ + NH_4^+: 1534.05 $[M + NH_4]^+$; observed 1534.50; m/z calculated for $C_{80}H_{135}N_3O_{18}$ + H^+: 1426.98 [M-benzyl + H]$^+$; observed 1426.58; m/z calculated for $C_{73}H_{129}N_3O_{18}$ + H^+: 1336.94 [M-2benzyl + H]$^+$; observed 1336.58; m/z calculated for

$C_{66}H_{123}N_3O_{18}$ + H^+: 1246.89 [M-3benzyl + H]$^+$; observed 1246.58; *m*/*z* calculated for $C_{87}H_{141}N_3O_{18}$ + 2(NH_4^+): 776.04 [M + 2NH_4]$^{2+}$; observed 776.33; *m*/*z* calculated for $C_{80}H_{135}N_3O_{18}$ + NH_4^+ + H: 722.51 [M-benzyl + NH_4 + H]$^{2+}$; observed 772.75; *m*/*z* calculated for $C_{87}H_{141}N_3O_{18}$ + 2(NH_4^+) + H^+: 517.70 [M + 2NH_4 + H]$^{3+}$; observed 517.75.

iBTA-C_{11}-EG_4. A round-bottom flask was charged with **17** (42.2 mg, 0.027 mmol) in MeOH (10 mL) and flushed with N_2 gas for 10 minutes. 10% Pd/C (6.3 mg) was subsequently added, followed by H_2 exchange facilitated with a balloon. The mixture was left stirring overnight under H_2 atmosphere. Afterwards, a small amount of the reaction mixture was taken and filtered over Celite in a Pasteur pipette to check conversion using ^{1}H NMR. After confirmation of full deprotection, the rest of the mixture was filtered through Celite which was washed with MeOH until TLC did not show any UV-active spots. The combined organic phases were concentrated *in vacuo* and the material was obtained as a brown waxy solid. Yield: 19.877 mg, 59%. ^{1}H NMR (400 MHz, $CDCl_3$ δ): 9.32 (m, 1H, ArN$\underline{H}$COCH$_2$), 8.24 (s, 2H, core protons), 7.98 (s, 1H, core proton between regular amides), 7.12 (m, 2H, 2× ArCON$\underline{H}$CH$_2$), 3.69–3.62 (m, 48H, O(C$\underline{H}_2$)$_2$O), 3.47–3.38 (m, 10H, 3× CH$_2$CH$_2$C$\underline{H}_2$O, 2× CONHC$\underline{H}_2$CH$_2$), 2.43–2.39 (t, J = 7.5 Hz, ArNHOCC$\underline{H}_2$CH$_2$), 1.73–1.68 (m, 2H, ArNHOCCH$_2$C$\underline{H}_2$), 1.60–1.53 (m, 10H, 3× CH$_2$C$\underline{H}_2$CH$_2$O, 2× ArCONHCH$_2$C$\underline{H}_2$), 1.36–1.21 (m, 42H, aliphatic). ^{13}C NMR (100 MHz, $CDCl_3$ δ): 173.00, 166.78, 139.34, 135.45, 120.89, 72.55, 71.54, 70.49, 70.45, 70.37, 70.34, 70.10, 69.82, 61.46, 40.30, 37.34, 29.62, 29.44, 29.40, 29.36, 29.33, 29.19, 26.92, 25.96, 25.47. FT-IR (ATR) ν (cm^{-1}): 3460, 3346, 3074, 2927, 2853, 1729, 1656, 1595, 1546, 1460, 1428, 1346, 1286, 1244, 1106, 943, 882, 837, 707, 697. MALDI-TOF-MS: *m*/*z* calculated for $C_{66}H_{123}N_3O_{18}$ + Na^+: 1268.87 [M + Na]$^+$; observed 1268.69; *m*/*z* calculated for $C_{66}H_{123}N_3O_{18}$ + K^+: 1284.98 [M + K]$^+$; observed 1284.85.

5-Amino-N_1,N_3-bis(1-phenyl-2,5,8,11,14-pentaoxahexacosan-26-yl)isophthalamide (1). A round-bottom flask was charged with 5-aminoisophthalic acid (0.1994 g, 1.1007 mmol) in thionyl chloride (15 mL). The mixture was stirred at room temperature for one hour, after which it was left to reflux for two hours. Conversion was checked using FT-IR and after two hours, no broad peak corresponding to a carboxylic acid could be seen anymore. The mixture was concentrated *in vacuo*, co-evaporated with toluene once and used without further purification. Subsequently, a two-necked round bottom flask was dried at 140 °C and charged with **7b** (1.08 g, 2.30 mmol) in dry THF (15 mL). Triethylamine (420.0 μL, 3.0 mmol) was added in one portion and the mixture was stirred for 20 min. The flask was cooled to 0 °C and the acid-chloride was dissolved in dry THF (10 mL) and added dropwise. The mixture was stirred overnight at RT, after which it was concentrated *in vacuo*. The mixture was dissolved in chloroform and extracted with water (3× 20 mL). The combined aqueous phases were washed with chloroform (3× 50 mL) and the combined organic phases were dried over $MgSO_4$ and concentrated *in vacuo*. The mixture was purified using column chromatography (SNAP-KI column 12 g, eluent DCM/methanol 95/5) and obtained as a dark yellow oil. Hereafter, it was determined that impurities were still present using LC-MS. Therefore, reversed phase column was used to obtain the pure product (C_{18} column 30 g, eluent acetonitrile/water 3 CV ramp 1/9–5/5; 4 CV 5/5; 1 CV ramp to 6/4; 1 CV 6/4; 1 CV ramp to 7/3; 5 CV 7/3; 1 CV ramp to 8/2; 14 CV 8/2). After freeze-drying, the material was obtained as an off-white flaky solid. Yield: 290.3 mg, 25%. ^{1}H NMR (400 MHz, $CDCl_3$ δ): 7.45 (s, 1H, core), 7.34–7.27 (m, 10H, Ar), 7.22 (s, 2H, core), 6.30 (s, 2H, 2× ArCON$\underline{H}$CH$_2$), 4.57 (s, 4H, ArC$\underline{H}_2$O), 3.68–3.62 (m, 28H, O(C$\underline{H}_2$)$_2$O), 3.58–3.56 (m, 4H, O(C$\underline{H}_2$)$_2$O), 3.45–3.38 (m, 8H, CH$_2$CH$_2$C$\underline{H}_2$O, ArCONHC$\underline{H}_2$CH$_2$CH$_2$), 1.60–1.54 (m, 8H, CH$_2$C$\underline{H}_2$CH$_2$O, ArCONHCH$_2$C$\underline{H}_2$CH$_2$), 1.38–1.26 (m, 32H, aliphatic). ^{13}C NMR (100 MHz, $CDCl_3$ δ): 128.36, 127.76, 127.60, 77.21, 73.26, 71.54, 70.63, 70.06, 29.60, 29.49, 29.44, 29.43, 29.42, 29.40, 29.23, 26.05. FT-IR (ATR) ν (cm^{-1}): 3322, 2924, 2854, 1619, 1593, 1524, 1454, 1348, 1291, 1100, 860, 732, 698. LC-MS: Calculated M_w: *m*/*z* calculated for $C_{62}H_{101}N_3O_{12}$ + H^+: 1080.75 [M + H]$^+$; observed 1080.58; *m*/*z* calculated for $C_{62}H_{101}N_3O_{12}$ + H^++Na^+: 551.87 [M + H + Na]$^{2+}$; observed 551.75; *m*/*z* calculated for $C_{55}H_{95}N_3O_{12}$ + H^+: 990.70 [M-benzyl + H]$^+$; observed 990.58.

5-(1-Phenyl-2,5,8,11,14-pentaoxaheptacosan-27-amido)-N_1, N_3-bis(1-phenyl-2,5,8,11,14-pentaoxahexacosan-26-yl)isophthalamide (2). An oven-dried round-bottom flask (dried at 140 °C) was charged with **11b** (138.9 mg, 0.3 mmol) in DCM (5 mL). Oxalyl chloride (150.0 μL, 1.7 mmol) was added to the stirring mixture. One droplet DMF was added, after which vigorous bubbling was observed. After ten minutes, a bright yellow colour was observed. The mixture was left to stir for three hours, after which it was concentrated *in vacuo*. The conversion of the carboxylic acid was confirmed using ^{1}H NMR and it was used without further purification. Subsequently, a two-necked round bottom flask (dried at 140 °C) was charged with **1** (190.2 mg, 0.2 mmol) in dry THF (15 mL). Triethylamine (200.0 μL, 1.6 mmol) was added in one portion and the mixture was stirred for 15 min. The acid chloride was dissolved in dry THF (10 mL) and added dropwise. The mixture was stirred overnight, after which it was concentrated *in vacuo*. The mixture was purified using column chromatography (SNAP-KI 12 g, eluent isopropanol/DCM 4/96). After this, LC-MS still showed impurities, so a reversed phase column was performed (C_{18} column 30 g, eluent acetonitrile/water 2 CV ramp 1/9–5/5; 2 CV 5/5; 1 CV ramp to 7/3; 2 CV 7/3; 1 CV ramp to 8/2; 2.5 CV 8/2; 1 CV ramp to 9/1; 3.7 CV 9/1; 2 CV ramp to 10/0; 7.7 CV 10/0; 1 CV ramp to 1/9; 2.8 CV 1/9; 1 CV ramp to 10/0; 12.7 CV 10/0). The acetonitrile was removed *in vacuo* and the product was obtained after lyophilization as a white solid (205 mg, 74%).

^{1}H NMR (400 MHz, $CDCl_3$ δ): 8.19 (s, 2H, core protons), 7.93 (s, 1H, core proton), 7.73 (m, 1H, ArN$\underline{H}$COCH$_2$), 7.34–7.27 (m, 15H, Ar), 6.39 (m, 2H, 2× ArCON$\underline{H}$CH$_2$), 4.56 (s, 6H, ArC$\underline{H}_2$O), 3.69–3.62 (m, 42H, O(C$\underline{H}_2$)$_2$O), 3.57–3.55 (m, 6H, O(C$\underline{H}_2$)$_2$O), 3.47–3.38 (m, 10H, 3× CH$_2$CH$_2$C$\underline{H}_2$O, 2× ArCONHC$\underline{H}_2$CH$_2$), 2.43–2.39 (t, J = 7.5 Hz, 2H, ArNHCOC$\underline{H}_2$CH$_2$), 1.73–1.67 (m, 2H, 1.85 ArNHCOCH$_2$C$\underline{H}_2$),

1.60–1.53 (m, 10H, 3× $CH_2C\underline{H}_2CH_2O$, 2× $ArNHCOCH_2C\underline{H}_2$), 1.36–1.21 (m, 48H, aliphatic). ^{13}C NMR (100 MHz, $CDCl_3$ δ): 128.36, 127.76, 127.60, 77.22, 73.25, 71.55, 70.66, 70.61, 70.05, 69.44, 64.45, 29.48, 29.23, 26.93, 26.07, 25.37. FT-IR (ATR) ν (cm^{-1}): 3315, 2924, 2854, 1642, 1536, 1451, 1349, 1293, 1247, 1104, 749, 698. LC-MS: *m*/*z* calculated for $C_{90}H_{147}N_3O_{18}$ + H^+: 1559.08 $[M + H]^+$; observed 1558.83; *m*/*z* calculated for $C_{77}H_{137}N_3O_{18}$ + H^+: 1393.00 [M-2benzyl + H]$^+$; observed 1378.75; *m*/*z* calculated for $C_{90}H_{147}N_3O_{18}$ + 2(Na^+): 802.03 $[M + 2Na]^{2+}$; observed 802.25; *m*/*z* calculated for $C_{90}H_{147}N_3O_{18}$ + 3(Na^+): 542.35 $[M + 3Na]^{3+}$; observed 542.75.

iBTA-C_{12}-EG_4. The synthesis of **iBTA-C_{12}-EG_4** was performed following the same procedure as described for **iBTA-C_{11}-EG_4**, yielding **iBTA-C_{12}-EG_4** as a white solid. Yield: 134.1 mg, 80%. ^1H NMR (400 MHz, $CDCl_3$ δ): 8.28 (m, 1H, $ArN\underline{H}COCH_2$), 8.22 (s, 2H, core protons), 7.95 (s, 1H, core proton between regular amides), 6.61 (m, 2H, 2× $ArCONH\underline{C}H_2$), 3.69–3.62 (m, 48H, $O(C\underline{H}_2)_2O$), 3.47–3.38 (m, 10H, 3× $CH_2CH_2C\underline{H}_2O$, 2× $ArCONHC\underline{H}_2CH_2$), 2.43–2.39 (t, J = 7.5 Hz, 2H, 2× $ArNHCOC\underline{H}_2CH_2$), 1.73–1.68 (m, 2H, $ArNHCOCH_2C\underline{H}_2$), 1.60–1.53 (m, 10H, 3× $CH_2C\underline{H}_2CH_2O$, 2× $ArCONHCH_2C\underline{H}_2$), 1.36–1.21 (m, 48H, aliphatic). ^{13}C NMR (100 MHz, $CDCl_3$ δ): 172.60, 166.46, 139.23, 135.60, 120.62, 72.64, 71.57, 71.55, 70.62, 70.60, 70.56, 70.53, 70.27, 70.03, 61.69, 40.30, 37.49, 29.52, 29.46, 29.44, 29.40, 29.37, 29.35, 29.31, 29.22, 26.92, 26.04, 26.00, 25.43. FT-IR (ATR) ν (cm^{-1}): 3608–3068, 2924, 2854, 1637, 1603, 1546, 1444, 1335, 1272, 1118, 935, 884, 721. LC-MS: *m*/*z* calculated for $C_{69}H_{129}N_3O_{18}$ + H^+: 1288.84 $[M + H]^+$; observed 1288.67; *m*/*z* calculated for $C_{69}H_{129}N_3O_{18}$ + 2(H^+): 644.98 $[M + 2H]^{2+}$; observed 944.92; *m*/*z* calculated for $C_{69}H_{129}N_3O_{18}$ + 3(H^+): 430.32 $[M + 3H]^{3+}$; observed 430.58.

5-Amino-N_1,N_3-bis(1-hydroxy-3,6,9,12-tetraoxatetracosan-24-yl) isophthalamide (3). A round bottom flask (50 ml, dried at 140 °C) was charged with methanol (10 ml) and **1** (28.0 mg, 0.026 mmol). The solution was purged with N_2 gas for 10 minutes to ensure all atmospheric oxen was removed. 10% Pd/C catalyst (10 mg) was added and a balloon filled with H_2 gas was attached. The solution was saturated with hydrogen gas and the mixture was left to stir overnight at room temperature. A small aliquot was taken and filtered over Celite to check using TLC for conversion (Hept : EtAc 50 : 50). Hereafter, the mixture was filtered over Celite and concentrated *in vacuo* to obtain the product as a white solid. Yield: 18.6 mg, 80%. ^1H NMR (400 MHz, $CDCl_3$ δ): 7.51 (s, 1H, core), 7.20 (s, 2H, core), 6.71 (s, 2H, 2× $ArCONH\underline{C}H_2$), 3.72–3.57 (m, 32H, $O(C\underline{H}_2)_2O$), 3.44–3.36 (m, 8H, $CH_2CH_2C\underline{H}_2O$, $ArCONHC\underline{H}_2CH_2CH_2$), 1.58–1.54 (m, 8H, $CH_2C\underline{H}_2CH_2O$, $ArCONHCH_2C\underline{H}_2CH_2$), 1.38–1.24 (m, 32H, aliphatic). ^{13}C NMR (100 MHz, DMSO-d_6 δ): 79.79, 79.46, 79.13, 72.81, 70.80, 70.30, 70.28, 70.25, 69.95, 60.65, 29.69, 29.52, 29.50, 29.37, 29.24, 26.83, 26.13. FT-IR (ATR) ν (cm^{-1}): 3298, 2925, 2855, 1640, 1555, 1462, 1348, 1312, 1250, 1208, 1102, 941, 884. MALDI-TOF-MS: *m*/*z* calculated for $C_{48}H_{89}N_3O_{12}$ + Na^+: 922.63 $[M + Na]^+$; observed 922.66; *m*/*z* calculated for $C_{48}H_{89}N_3O_{12}$ + K^+: 938.74 $[M + K]^+$; observed 938.62.

iBTA-C_{12}-EG_4-N_3 (4). A 10 mL round bottom flask was charged with **3** (crude mixture, 100 mg), **14** (44.8 mg, 0.103 mmol) and 3 mL MeOH. To this, DMT-MM (62.0 mg, 0.224 mmol) was added and the mixture was stirred overnight. Hereafter, the reaction was not complete hence more DMT-MM (43.3 mg, 0.156 mmol) was added and the mixture was stirred overnight again. The mixture was concentrated *in vacuo* and purified using reversed phase column (C_{18} column 30 g, eluent acetonitrile/water 3 CV ramp 1/9–5/5; 2 CV 5/5; 1 CV ramp to 6/4; 2 CV 6/4; 1 CV ramp to 7/3; 2 CV 7/3; 1 CV ramp to 8/2; 2CV 8/2; 1 CV ramp to 9/1; 1 CV 9/1; 1 CV ramp to 9.5/0.5; 2 CV 9.5/0.5) to obtain the product as a white solid. Yield: 33.8 mg, 23%. ^1H NMR (400 MHz, $CDCl_3$ δ): 8.20 (s, 2H, core protons), 8.14 (s, 1H, $ArN\underline{H}COCH_2$), 7.95 (s, 1H, core proton between regular amides), 6.59 (s, 2H, 2× $ArCONH\underline{C}H_2$), 3.72–3.57 (m, 48H, $O(C\underline{H}_2)_2O$), 3.44–3.37 (m, 12H, 3× $CH_2CH_2C\underline{H}_2O$, 2× $ArCONHC\underline{H}_2CH_2$, $OCH_2C\underline{H}_2N_3$), 2.41 (t, J = 8.0 Hz, 2H, $NHCOC\underline{H}_2$), 1.72–1.53 (water influence, m, 12H, 1× $NHCOCH_2C\underline{H}_2CH_2$, 2× $CONHCH_2C\underline{H}_2CH_2$, 3× $C\underline{H}_2CH_2O(CH_2)_2O$), 1.37–1.16 (m, 48H, aliphatic chain). ^{13}C NMR (100 MHz, $CDCl_3$ δ): 172.43, 166.30, 139.11, 135.63, 120.52, 77.34, 77.02, 76.70, 72.62, 71.57, 70.70, 70.64, 70.61, 70.55, 70.52, 70.27, 70.06, 70.03, 70.01, 61.70, 50.69, 40.28, 37.58, 29.61, 29.53, 29.51, 29.49, 29.43, 29.37, 29.26, 29.15, 26.87, 26.06, 26.03, 25.44. FT-IR (ATR) ν (cm^{-1}): 3464, 3305, 2926, 2856, 2102, 1643, 1594, 1539, 1441, 1346, 1278, 1109, 942, 888. LC-MS: *m*/*z* calculated for $C_{69}H_{128}N_6O_{17}$ + H^+: 1313.94 $[M + H]^+$; observed 1313.58; *m*/*z* calculated for $C_{69}H_{128}N_6O_{17}$ + Na^+: 1335.92 $[M + Na]^+$; observed 1335.83; *m*/*z* calculated for $C_{69}H_{128}N_6O_{17}$ + 2(H^+): 657.48 $[M + 2H]^{2+}$; observed 657.33; *m*/*z* calculated for $C_{69}H_{128}N_6O_{17}$ + H^+ + Na^+: 668.47 $[M + H + Na]^{2+}$; observed 668.42; *m*/*z* calculated for $C_{69}H_{128}N_6O_{17}$ + 2(Na^+): 679.46 $[M + 2Na]^{2+}$; observed 679.50.

iBTA-C_{12}-EG_4-Cy3. A 5 mL round bottom flask was charged with **4** (4.6 mg, 0.0035 mmol) and alkyne-sulfo-Cy3 (5.0 mg, 0.0072 mmol) in 1 mL DMSO. To this mixture, $CuSO_4$ (1.117 mg, 0.0070 mmol) and Na-L-ascorbate (1.370 mg, 0.0069 mmol) were added in a minimal amount of water. The mixture was stirred at RT overnight. LC-MS showed conversion of the starting material, thus the mixture was concentrated *in vacuo*. Subsequently the crude mixture was dissolved in $CHCl_3$ and extracted three times with water. The organic fraction was dried over $MgSO_4$ and concentrated *in vacuo* to obtain the product as a bright pink solid. Yield: 4.0 mg, 58%. LC-MS: *m*/*z* calculated for $C_{102}H_{166}N_9O_{24}S_2^-$ + H^++2(Na^+): 1005.57 $[M + H + 2Na]^{2+}$; observed 1006.67; *m*/*z* calculated for $C_{102}H_{166}N_9O_{24}S_2^-$ + 4(H^+): 656.40 $[M + 4H]^{3+}$; observed 656.75.

Author contributions

S. M. C. S., B. W. L. B., L. S. and A. R. A. P. planned the experiments. S. M. C. S., B. W. L. B. and S. D. carried out the experiments. S. M. C. S., B. W. L. B. and A. R. A. P. wrote the manuscript. All the authors have read and agreed to the published version of the manuscript.

Conflicts of interest

There are no conflicts to declare.

Acknowledgements

This work was supported by the Dutch Ministry of Education, Culture and Science (Gravity program 024.001.035) and the European Research Council (H2020-EU.1.1., SYNMAT project, ID 788618). A. J. H. Spiering and Nicholas Matsumoto are gratefully acknowledged for the synthesis of **BTA-C_{11}-EG_4** and **BTA-C_{12}-EG_4**. Svenja Herziger and Christoph Böttcher are gratefully acknowledged for their support in the structural characterization of **BTA-C_{11}-EG_4**. We would like to thank E. W. Meijer for fruitful discussions.

References

1 C. Sanchez, H. Arribart and M. M. G. Guille, *Nat. Mater.*, 2005, **4**, 277–288.
2 T. P. J. Knowles, M. Vendruscolo and C. M. Dobson, *Nat. Rev. Mol. Cell Biol.*, 2014, **15**, 384–396.
3 D. A. Fletcher and R. D. Mullins, *Nature*, 2010, **463**, 485–492.
4 D. Lingwood and K. Simons, *Science*, 2010, **327**, 46–50.
5 O. J. G. M. Goor, S. I. S. Hendrikse, P. Y. W. Dankers and E. W. Meijer, *Chem. Soc. Rev.*, 2017, **46**, 6621–6637.
6 E. Krieg, M. M. C. Bastings, P. Besenius and B. Rybtchinski, *Chem. Rev.*, 2016, **116**, 2414–2477.
7 P. Y. W. Dankers, M. C. Harmsen, L. A. Brouwer, M. J. A. Van Luyn and E. W. Meijer, *Nat. Mater.*, 2005, **4**, 568–574.
8 K. Petkau-Milroy, M. H. Sonntag and L. Brunsveld, *Chem. – Eur. J.*, 2013, **19**, 10786–10793.
9 R. N. Shah, N. A. Shah, M. M. Del Rosario Lim, C. Hsieh, G. Nuber and S. I. Stupp, *Proc. Natl. Acad. Sci. U. S. A.*, 2010, **107**, 3293–3298.
10 A. Mata, Y. Geng, K. J. Henrikson, C. Aparicio, S. R. Stock, R. L. Satcher and S. I. Stupp, *Biomaterials*, 2010, **31**, 6004–6012.
11 N. A. Mansukhani, E. B. Peters, M. M. So, M. S. Albaghdadi, Z. Wang, M. R. Karver, T. D. Clemons, J. P. Laux, N. D. Tsihlis, S. I. Stupp and M. R. Kibbe, *Macromol. Biosci.*, 2019, **19**, 1900066.
12 R. Mammadov, B. Mammadov, S. Toksoz, B. Aydin, R. Yagci, A. B. Tekinay and M. O. Guler, *Biomacromolecules*, 2011, **12**, 3508–3519.
13 S. I. S. Hendrikse, S. P. W. Wijnands, R. P. M. Lafleur, M. J. Pouderoijen, H. M. Janssen, P. Y. W. Dankers and E. W. Meijer, *Chem. Commun.*, 2017, **53**, 2279–2282.
14 M. H. Bakker, R. E. Kieltyka, L. Albertazzi and P. Y. W. Dankers, *RSC Adv.*, 2016, **6**, 110600–110603.
15 R. C. van Gaal, B. D. Ippel, S. Spaans, M. I. Komil and P. Y. W. Dankers, *J. Polym. Sci.*, 2021, 1–14.
16 D. Straßburger, N. Stergiou, M. Urschbach, H. Yurugi, D. Spitzer, D. Schollmeyer, E. Schmitt and P. Besenius, *ChemBioChem*, 2018, **19**, 912–916.
17 K. Petkau-Milroy, M. H. Sonntag, A. H. A. M. van Onzen and L. Brunsveld, *J. Am. Chem. Soc.*, 2012, **134**, 8086–8089.
18 K. Petkau-Milroy, M. H. Sonntag, A. Colditz and L. Brunsveld, *Int. J. Mol. Sci.*, 2013, **14**, 21189–21201.
19 M. K. Müller, K. Petkau and L. Brunsveld, *Chem. Commun.*, 2011, **47**, 310–312.
20 S. Cantekin, T. F. A. de Greef and A. R. A. Palmans, *Chem. Soc. Rev.*, 2012, **41**, 6125.
21 P. J. M. Stals, J. C. Everts, R. De Bruijn, I. A. W. Filot, M. M. J. Smulders, R. Martín-Rapún, E. A. Pidko, T. F. A. De Greef, A. R. A. Palmans and E. W. Meijer, *Chem. – Eur. J.*, 2010, **16**, 810–821.
22 J. Van Herrikhuyzen, P. Jonkheijm, A. P. H. J. Schenning and E. W. Meijer, *Org. Biomol. Chem.*, 2006, **4**, 1539–1545.
23 C. M. A. Leenders, L. Albertazzi, T. Mes, M. M. E. Koenigs, A. R. A. Palmans and E. W. Meijer, *Chem. Commun.*, 2013, **49**, 1963–1965.
24 C. M. A. Leenders, M. B. Baker, I. A. B. Pijpers, R. P. M. Lafleur, L. Albertazzi, A. R. A. Palmans and E. W. Meijer, *Soft Matter*, 2016, **12**, 2887–2893.
25 X. Lou, R. P. M. Lafleur, C. M. A. Leenders, S. M. C. Schoenmakers, N. M. Matsumoto, M. B. Baker, J. L. J. van Dongen, A. R. A. Palmans and E. W. Meijer, *Nat. Commun.*, 2017, **8**, 15420.
26 X. Lou, S. M. C. Schoenmakers, J. L. J. van Dongen, M. Garcia-Iglesias, N. M. Casellas, M. Fernández-Castaño Romera, R. P. Sijbesma, E. W. Meijer and A. R. A. Palmans, *J. Polym. Sci.*, 2021, **59**, 1151–1161.
27 B. N. S. Thota, X. Lou, D. Bochicchio, T. F. E. Paffen, R. P. M. Lafleur, J. L. J. van Dongen, S. Ehrmann, R. Haag, G. M. Pavan, A. R. A. Palmans and E. W. Meijer, *Angew. Chem., Int. Ed.*, 2018, **57**, 6843–6847.
28 G. Morgese, B. F. M. Waal, S. Varela-Aramburu, A. R. A. Palmans, L. Albertazzi and E. W. Meijer, *Angew. Chem.*, 2020, **59**, 17382–17386.
29 M. H. Bakker, C. C. Lee, E. W. Meijer, P. Y. W. Dankers and L. Albertazzi, *ACS Nano*, 2016, **10**, 1845–1852.
30 S. I. S. Hendrikse, L. Su, T. P. Hogervorst, R. P. M. Lafleur, X. Lou, G. A. van der Marel, J. D. C. Codee and E. W. Meijer, *J. Am. Chem. Soc.*, 2019, **141**, 13877–13886.
31 S. P. W. Wijnands, W. Engelen, R. P. M. Lafleur, E. W. Meijer and M. Merkx, *Nat. Commun.*, 2018, **9**, 65.
32 K. Petkau-Milroy and L. Brunsveld, *Eur. J. Org. Chem.*, 2013, 3470–3476.
33 J. Roosma, T. Mes, P. Leclère, A. R. A. Palmans and E. W. Meijer, *J. Am. Chem. Soc.*, 2008, **130**, 1120–1121.
34 J. J. Van Gorp, J. A. J. M. Vekemans and E. W. Meijer, *Mol. Cryst. Liq. Cryst.*, 2003, **397**, 191–205.
35 S. Bera, S. K. Maity and D. Haldar, *CrystEngComm*, 2014, **16**, 4834–4841.
36 N. San-José, A. Gómez-Valdemoro, S. Ibeas, F. C. García, F. Serna and J. M. García, *Supramol. Chem.*, 2010, **22**, 325–338.

37 S. Kumar, S. Bera, S. K. Nandi and D. Haldar, *Soft Matter*, 2021, **17**, 113–119.
38 M. U. Kassack, K. Braun, M. Ganso, H. Ullmann, P. Nickel, B. Böing, G. Müller and G. Lambrecht, *Eur. J. Med. Chem.*, 2004, **39**, 345–357.
39 M. Blomenhofer, S. Ganzleben, D. Hanft, H. W. Schmidt, M. Kristiansen, P. Smith, K. Stoll, D. Mäder and K. Hoffmann, *Macromolecules*, 2005, **38**, 3688–3695.
40 Y. Zhou, M. Xu, T. Yi, S. Xiao, Z. Zhou, F. Li and C. Huang, *Langmuir*, 2007, **23**, 202–208.
41 F. V. Gruschwitz, M. C. Fu, T. Klein, R. Takahashi, T. Higashihara, S. Hoeppener, I. Nischang, K. Sakurai and J. C. Brendel, *Macromolecules*, 2020, **53**, 7552–7560.
42 Y. Li, L. Dubreucq, B. G. Alvarenga, M. Raynal and L. Bouteiller, *Chem. – Eur. J.*, 2019, **25**, 10650–10661.
43 M. J. Rust, M. Bates and X. Zhuang, *Nat. Methods*, 2006, **3**, 793–795.
44 B. Huang, M. Bates and X. Zhuang, *Annu. Rev. Biochem.*, 2009, **78**, 993–1016.
45 L. Albertazzi, D. van der Zwaag, C. M. A. Leenders, R. Fitzner, R. W. van der Hofstad and E. W. Meijer, *Science*, 2014, **344**, 491–495.
46 R. M. P. Da Silva, D. Van Der Zwaag, L. Albertazzi, S. S. Lee, E. W. Meijer and S. I. Stupp, *Nat. Commun.*, 2016, **7**, 1–10.
47 S. Pujals, N. Feiner-Gracia, P. Delcanale, I. Voets and L. Albertazzi, *Nat. Rev. Chem.*, 2019, **3**, 68–84.
48 L. Albertazzi, F. J. Martinez-Veracoechea, C. M. A. Leenders, I. K. Voets, D. Frenkel and E. W. Meijer, *Proc. Natl. Acad. Sci. U. S. A.*, 2013, **110**, 12203–12208.
49 M. Lange, A. L. Pettersen and K. Undheim, *Tetrahedron*, 1998, **54**, 5745–5752.
50 H. Sajiki, *Tetrahedron Lett.*, 1995, **36**, 3465–3468.
51 R. P. M. Lafleur, X. Lou, G. M. Pavan, A. R. A. Palmans and E. W. Meijer, *Chem. Sci.*, 2018, **9**, 6199–6209.
52 R. P. M. Lafleur, S. Herziger, S. M. C. Schoenmakers, A. D. A. Keizer, J. Jahzerah, B. N. S. Thota, L. Su, P. H. H. Bomans, N. A. J. M. Sommerdijk, A. R. A. Palmans, R. Haag, H. Friedrich, C. Böttcher and E. W. Meijer, *J. Am. Chem. Soc.*, 2020, **142**, 17644–17652.
53 T. Aiba, M. Sato, D. Umegaki, T. Iwasaki, N. Kambe, K. Fukase and Y. Fujimoto, *Org. Biomol. Chem.*, 2016, **14**, 6672–6675.